JAERI-M
9853

EXPERIMENTAL APPROACH TO HIGH-POWER LONG-DURATION NEUTRAL BEAMS

December 1981

Hiroshi HORIIKE

日本原子力研究所
Japan Atomic Energy Research Institute

JAERI-Mレポートは，日本原子力研究所が不定期に公刊している研究報告書です。
入手の問合わせは，日本原子力研究所技術情報部情報資料課（〒319-11茨城県那珂郡東海村）あて，お申しこしください。なお，このほかに財団法人原子力弘済会資料センター（〒319-11 茨城県那珂郡東海村日本原子力研究所内）で複写による実費頒布をおこなっております。

JAERI-M reports are issued irregularly.
Inquiries about availability of the reports should be addressed to Information Section, Division of Technical Information, Japan Atomic Energy Research Institute, Tokai-mura, Naka-gun, Ibaraki-ken 319-11, Japan.

©Japan Atomic Energy Research Institute, 1981

編集兼発行　日本原子力研究所
印　　刷　いばらき印刷㈱

JAERI-M 9853

Experimental Approach to High Power Long Duration Neutral Beams

Hiroshi HORIIKE

Division of Thermonuclear Fusion Research,
Tokai Research Establishment, JAERI

(Received November 26, 1981)

Experimental studies of ion sources and beam dumps for the development of a high power long duration neutral beam injector for JT-60 are presented. Long pulse operation of high power beams requires a high degree of reliability. To develop a reliable ion source with large extraction area, a new duoPIGatron ion source with a coaxially shaped intermediate electrode is proposed and tested. Magnetic configuration is examined numerically to obtain high current arc discharge and source plasma with small density variation. Experimental results show that primary electrons were fed widely from the cathode plasma region to the source plasma region and that dense uniform source plasma could be obtained easily. Source plasma characteristics are studied and comparison of these with other sources are also described. To develop extraction electrode of high power ion source, experimental studies were made on the cooling of the electrode. Long Pulse beams were extracted safely under the condition of high heat loading on the electrode. Finally, burnout study for the development of high power beam dumps is presented. Burnout data were obtained from subcooled forced-convective boiling of water in a copper finned tube irradiated by high power ion beams. The results yield simple burnout correlations which can be used for the prediction of burnout heat flux of the beam dump.

Keywords; Neutral Beam, Injector, Ion Source, Source Plasma , DuoPIGatron, Extraction Electrode, PIG Discharge, Burnout , JT-60

JAERI－M 9853

高出力長パルス中性粒子ビームへの実験的アプローチ

日本原子力研究所東海研究所核融合研究部
堀池　寛

（1981年11月26日受理）

本論文は高パワーで長い持続時間の中性粒子ビームを得るための実験研究についてまとめたものであり，イオン源とビームダンプの幾つかの問題を取扱った。高パワーで持続時間の長いビームを得るためにまず問題となるのはイオン源の信頼性であるが，これはソースプラズマ生成部やビーム引出し電極の堅牢さに左右される。ここでは信頼性の高い大型プラズマソースを得るため，中間電極を同軸形にした新しい形のデュオピガトロンイオン源を提案した。イオン源全体の磁場配位を数値計算によって計算することにより，一様な密度分布を持つソースプラズマを発生し且大電流で安定なアーク放電を可能とする磁場配位を求めた。試作モデルでの実験の結果，カソードプラズマ領域からソースプラズマ領域へ一次電子が広く供給されており，一様で高密度なソースプラズマが容易に得られることが示された。またソースプラズマの諸特性を磁場の効果を中心に検討し，他の形式のイオン源との比較を行った。次に高パワー長パルスビームを引出すことの可能な電極を得るため，強制冷却をした電極の実験を行った。電極の熱負荷を大きくした大型イオン源により近い条件の下で長い持続時間のビームを得ることができた。最後に高パワービームを受けるビームダンプを設計するため，イオンビームにて加熱した強制水冷銅管のバーンアウト熱流束を求める実験を行った。イオンビームなどにより冷却管が片側からのみ加熱される条件下でバーンアウトデータを求め，高パワービームにさらされる冷却管のバーンアウト熱流束をあらわす実験式を得た。

Contents

目　　次

1.1 REQUIREMENTS FOR NEUTRAL BEAM

For the achievement of the break-even condition in fusion plasmas it is necessary to satisfy two basic conditions: Plasma confinement and plasma heating. These conditions are represented by the Lawson criterion on plasma density and confinement time, as well as on the temperature. While a number of approaches for achieving these conditions have been tried, the main efforts have been narrowed down to the following four approaches: closed systems (tokamak, stellarator), open systems (mirror), theta pinch and laser-fusion.

In closed systems, fusion plasmas are confined by toroidally shaped magnetic lines of force which close within the system. Open systems utilizes magnetic mirrors which push back plasma particles outside the loss cone. Pinches are plasmas carrying large current which generate sufficient magnetic fields to confine and heat the plasma. In laser-fusion, the laser beams are focused onto a pellet or a gaseous column of DT to ignite, compress and heat it.

Among these approaches, the tokamak device originally developed in Soviet has been the most successful[1] and has received the highest attention. The tokamak alone has been capable of maintaining high temperature for appreciable energy confinement time. However, it becomes clear that the tokamak requires auxiliary heating to achieve break-even conditions[2].

Auxiliary heating is required because the ohmic resistance of the tokamak falls rapidly as the plasma temperature rises. Thus, the efficiency of ohmic heating decreases as higher plasma temperature are reached. Furthermore, stability requirements ($q > 1$) limit the maximum toroidal current that can be sustained in any particular tokamak. These two effects limit the maximum electron and hence ion temperatures that can be attained in a moderate field tokamak below several kilo-electron volts.

Thus, some auxiliary heating scheme is required to raise the plasma temperature to thermonuclear temperatures necessary for break-even and ignition. Once the plasma ignites, produced alpha particle will maintain the temperature and the auxiliary energy sources will no more be necessary. Although there exist many plasma heating mechanisms relevant to fusion (radio frequency, ohmic, compressional, shock, laser, electron-beam etc.), currently the most successful and thus most popular technique is a high power neutral beam injection. Neutral beam injection plays an important

role as a proven method of supplying auxiliary heat to a tokamak plasma in addition to its original application as a means of producing and sustaining an energetic plasma in mirror geometry[3]. This is also essential to the various types of suggested beam-fusion energy amplifier based on toroidal confinement[4),5)].

The principle of neutral injection is very simple. An intense high energy beam of neutral hydrogen (or hydrogen isotope) atoms is injected across the magnetic field and into the plasma. Here the energetic particles are ionized (mostly by charge exchange) and hence trapped in the magnetic field. They then slow down by multiple Coulomb collision with background ions and electrons, transfer their energy to the plasma and heat it.

The first neutral-beam injection experiment was performed on the CLEO tokamak (Culham) in late 1972, but the beam power was too small to produce measurable heating[6]. In 1973, significant ion heating was observed in the ATC device (Princeton)[7], the ORMAK device (Oak Ridge)[8], as well as in CLEO[9], with injected powers of 40-80 kW. By early 1976, ion temperature had been doubled to $\sim$2 keV in experiments on the ATC[10], ORMAK[11] and TFR (Fontenay-aux-Roses)[12] devices utilizing 200-500 kW injected power. In 1979 the Princeton Large Torus (PLT) experiment has achieved ion temperature above 6 keV[13]. The current optimistic prediction shows that scientific feasibility of fusion power will be achieved when large tokamaks such as JT-60, TFTR or JET[14] become operational in near future.

A fairly typical neutral beam injection system is shown in Fig. 1.1; which illustrates a general schematic of the 75 kV JT-60 neutral beam line[15]. The heart of the system is a high power ion source, where hydrogen ions are generated by diffuse arc discharge and are extracted and accelerated to the desired energy by a multi-electrode system. Extracted ions are subsequently neutralized by charge exchange interactions with background hydrogen gas in the neutralizer cell. Residual ions are removed from the neutral beam by a bending magnet in order to prevent severe beam line damage near the torus drift tube which will be caused by deflection of ions due to confinement field. Vacuum pumps provide isolation for the neutralizer cell and fusion plasma so that background pressure in the beam drift tube is insufficient to cause significant beam re-ionization.

The performance parameters of a neutral beam system must satisfy

stringent requirements set by engineering and physics considerations of the target plasma. Many of these parameters are mostly dependent on the properties of the ion source, beam handling ability of beam dumps and evacuation velocity of vacuum pump. Performance parameters for a single 75 kV JT-60 neutral beam line are listed in Table 1.1.

Beam energy requirements are primarily determined by the necessity of deposition of high energy neutrals well inside the target plasma, preferably near the center. The mean free path for beam ionization is propotional to the neutral energy and is inversely propotional to the plasma density, to the effective charge and to the neutral mass. Thus beam energy is a function of fusion plasma density, radius and impurity concentration. A beam energy of 75 keV is necessary for JT-60.

Beam current is determined from the total input power required to heat the fusion plasma. For JT-60, an input power of 20 MW is required. This translates into hundreds of amperes of injected current. However the demands on accelerated ion current are far more greater due to the low neutralization efficiency for proton beams at 75 keV as shown in Figs. 1.2 and 3. This, coupled with the dimension of injection ports, determines the individual source current. The large ion current with the high acceleration potential tends to cause large heat dissipation in the extraction electrodes of the ion source and in the ion dump for unneutralized beams.

Due to the molecular properties of hydrogen gas, the source plasma is composed of three main ion constituents: H^+, H_2^+ and H_3^+. Molecular dissociation for high energy collisions in the neutralizer cell, causes the H_2^+ and H_3^+ beam ions to dissociate into fractional energy atomic neutrals. A required species ratio for the JT-60 source is 75:20: 5 percent. However, a higher species ratio is preferable.

Beam divergence is limited by the configuration of the beam line. A drift duct must accommodate neutral beams as much as possible, while remaining small enough to fit through toroidal coils. On the other hand, beam lines are several meters long, e.g. 10 m for JT-60, in order to accommodate the beam line components such as the neutralizer cell, the bending magnet and the drift tube. Thus the beam divergence, defined in terms of the gaussian e-folding half width, must be less than one degree. These high convergent beams are produced with carefully shaped delicate electrode systems. The beam divergence is governed by several factors such as the electrostatic properties of the beam accelerator and ion

temperature of the source plasma. While for the acceleration potential of 75 keV two-stage acceleration system is employed, extracted beam current density j is principally related to electrode potential E and electrode spacing d through the Child-Langmuir relation of space-charge limited flow:

$$j \propto E^{3/2} / d^2$$

This indicates that maximum extracted ion current density for a constant potential, is limited by minimum of the spacing, which is limited by the threshold of electrical breakdowns. For the JT-60 ion source, the ion current density is designed to be 0.27 A/cm^2, which requires a grid area of 12 × 27 cm for the beam transparency of 40 %. This transparency is determined from the allowable space for cooling tubes of the electrodes. Each electrode must tolerate about 2 % of the beam power which is equivalent to the power loading of 50 kW.

For the production of high current ion beams with small beam divergence over the large extraction area, it is important to produce dense and quiescent source plasma with very small spatial density variations.

Pulse duration is determined in accordance with discharge duration of target plasma. Neutral beams for JT-60 are required to last up to 10 sec. This long pulse extraction of high power beams causes serious problems. One of the problems is cooling of the extraction electrodes. Because these electrodes are made thin and delicate to produce high convergent beams, it is difficult to maintain precisely adjusted electrode gaps and optical axes during long-pulse beam extraction. Another problem is the disposal of unneutralized ions. Heat load on a ion dump increases with beam energy. In addition the beams are focused very well, thus the incident power flux becomes very high, typically, as high as 100 MW/m^2 for the JT-60 neutral beam line. It is very difficult to handle such high power beams for long duration.

1.2 OUTLINE OF THE PRESENT WORK

The preceding discussion has illustrated the relation of overall beam performance to those of ion source and beam line components such as ion dump. In order to obtain neutral beams with high performance as

listed in Table 1.1, we must make efforts in studies of source plasma production, beam optics and long-pulse operation of ion source and ion dumps.

The following study is divided into two main parts. The first half presents a study of source plasma of a large extraction area. The latter half presents experimental approaches for long duration high power beams.

Long-pulse operation of the neutral beam injector with high duty cycle requires high degree of reliability of an ion source and an ion dump. Reliability of the ion source depends on lifetimes of the hot cathode and the extraction electrodes, which are the most fragile components of the source. The lifetime of the cathode is determined by the evaporation rate which increases rapidly with temperature in almost the same way as the emission current density. It is also limited by formation of hot spot which gives enhanced local emission and by the loss due to sputtering. In view of the cathode life those sources which operate with two discharge volumes (e.g. duoPIGatron) are superior to those which operate with a single plasma volume (e.g. magnetic multipole source, magnetic field free source) owing to lower cathode sheath potential and plasma density in the cathode region. In addition a duo-discharge source has smaller concentration of impurities in the beam.

The duoPIGatron, however, has one problem that electron emission from the primary plasma volume through the intermediate electrode is localized, leading to plasma non-uniformities. One method of overcoming this is to insert an axial copper button in the center of the discharge region. The button, however, destabilizes the arc discharge when the applied magnetic field is increased in order to raise the production efficiency of the source plasma. While the production efficiency is not a critical aspect of the overall beam line design, it impacts on source design and reliability in that low efficiency requires high arc currents and thus high cathode emission which limits lifetimes.

In chapter 2, we propose a new ion source in which primary electrons are fed widely to the PIG chamber by making use of the coaxially shaped intermediate electrode, and discuss the effect of the magnetic field configuration on the source plasma distribution. This source, named coaxial duoPIGatron ion source, has many advantages due to hollow feeding of electrons. Chapter 3 describes the detailed source plasma characteristics, especially the dependency of these on the magnetic field. Comparison with other source is also presented.

The other problem of an ion source is the maintenance of the electrostatic properties of the extraction electrodes. There is power lost by the beam in the extraction region due to collisions with the background gas, which produce electrode heating. For the JT-60 ion source the loading of electrodes need be only 2 % to produce 270 W/cm^2 on the grids. Since the grids are about 1.5 mm thick and have a transparency of 40 %, their thermal capacity is low and such power levels can produce high temperatures and consequent grid distortion leading to poor beam optics and grid destruction. Chapter 4 presents experiments on the power loading of the extraction electrodes and on the cooling system which can handle power loadings in the case of long-pulse beam extraction.

High power ion beams extracted from the ion source are converted to neutral particles in the gas cell. In most beam lines the non-neutralized ions are magnetically deflected and dumped on water cooled plates. As the total power level and pulse length are increased the problem of absorbing the power becomes more severe, together with the problem of pumping gas released by impact of the beam on the dump surface. To satisfy these requirements, the ion dump of the JT-60 neutral beam line consists of arrays of finned tubes. A reliable estimate of burnout heat flux is required for the design of the dump with thin wall cooling tubes. Thus we conducted an experimental study of burnout heat flux by means of high power long-pulse ion beams, which is described in chapter 5.

Chapter 6 presents the summary and conclusion.

References

1) L.A. Artsimovich, Nucl. Fusion 12 (1972) 215
2) J.G. Cordey, 3rd International Meeting on Theoretical and Experimental Aspects of Heating of Toroidal Plasmas, Grenoble, 28 June (1976)
3) F.H. Coensgen, UCRL-78057
4) J.G. Cordey and W.G.F. Core, Nucl. Fusion 15 (1975) 710
5) D.L. Jassby, Nucl. Fusion 17 (1977) 309
6) A. Gibson, et al., 3rd International Symposium in Toroidal Plasma Confinement, Garching, 1973, B16-1
7) K. Bol, et al., Phys. Rev. Lett. 32 (1974) 661
8) L.A. Berry, et al., 5th International Conference in Plasma Physics and Controlled Nuclear Fusion Research, Tokyo (1974) 1-113
9) J.G. Corday, et al., Nucl. Fusion 15 (1975) 441
10) R.A. Ellis, et al., Nucl. Fusion 16 (1976) 524
11) L.A. Berry, et al., 6th International Conference in Plasma Physics and Controlled Nuclear Fusion Research, Berchtesgaden, (1976) 1-49
12) TFR Group, 3rd International Meeting on Theoretical and Experimental Aspects of Heating of Toroidal Plasmas, Grenoble, 28 June (1976) 2-141
13) H. Eubank, et al., Phys. Rev. Lett. 43 (1979) 270
14) D.L. Jassby, Nucl. Fusion, 17 (1977) 373
15) S. Matsuda, et al., Japan Atomic Energy Research Institute Report JAERI-M 7655 (1978)

Table 1.1 Neutral Beam Requirements for JT-60 (single source)

Neutral Gas	Hydrogen
Beam Energy	75 kV
Beam Current	35 A
Beam Current Density	0.27 A/cm^2
Pulse Duration	10 sec
Grid Transparency	0.4
Source Extraction Area	12 × 27 cm^2
Beam Divergence Angle (1/e)	1.0°
Species Ratio (H^+:H_2^+:H_3^+)	75:20:5
Number of Sources	28

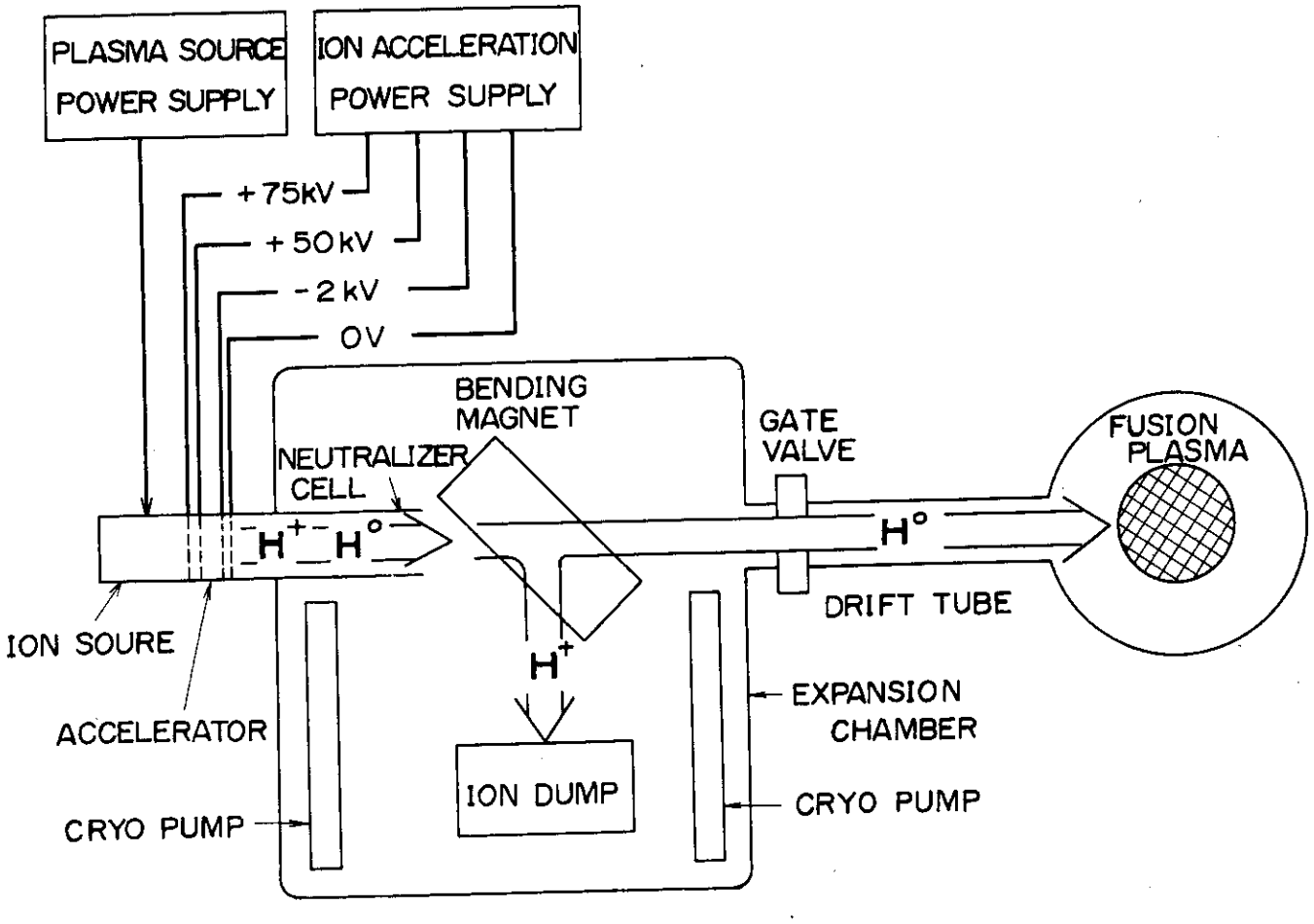

Fig. 1.1 75 kV neutral beam injection line for JT-60

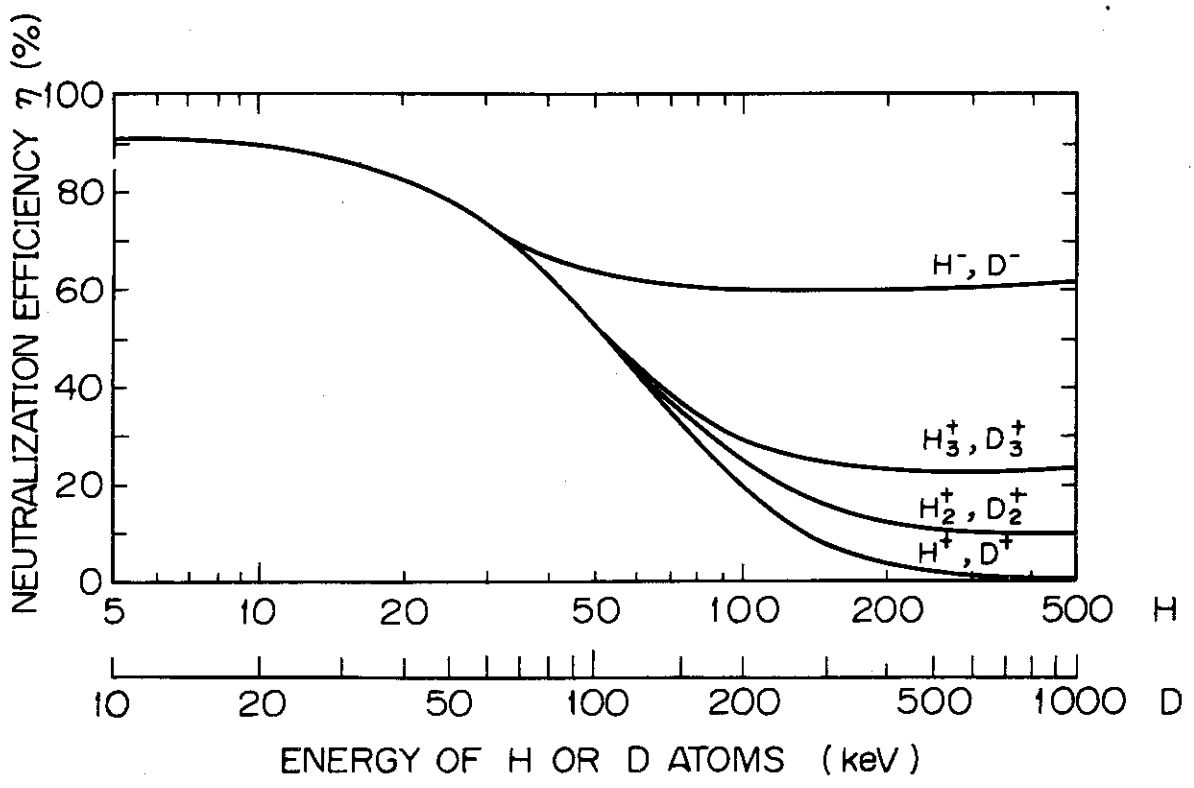

Fig. 1.2 Energy dependence of neutralization efficiency

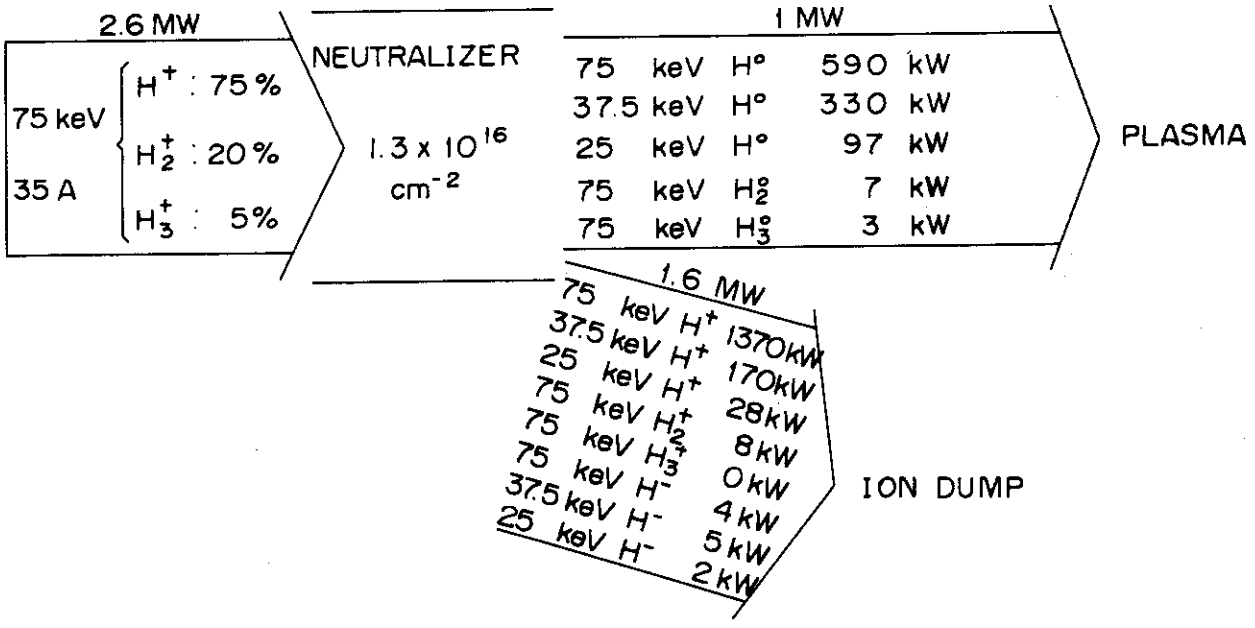

Fig. 1.3 Power and particle flow of 75 kV beam line

2.1 INTRODUCTION

A high power high current ion source is required to heat a large and dense plasma of the fusion experimental devices such as JT-60, TFTR or JET. The duoPIGatron ion source is one of such ion sources with the highest performance. It gives high proton ratio, excellent reliability[1] and small impurity contents[2]. However, uniformity of the source plasma generally becomes poor with an increase of the beam extraction area due to concentration of primary electrons to the central region.

There are some methods of improving the spatial density uniformity of the duoPIGatron ion source. One method is to insert an axial button in the center of the discharge region[3]. While the button can be easily attached to the ion source, it destabilizes the arc discharge when the source magnetic field is increased[4]. This is because the discharge electrons are difficult to diffuse across the magnetic lines of force that penetrate the button.

In the present chapter we report on another method of improving the spatial density uniformity. We employ a coaxially formed intermediate electrode to obtain hollow feeding of primary ionizing electrons to the PIG-chamber. In this case, most electrons are released along the diverging magnetic lines of force toward off-axis region of the PIG-chamber. It is easy to change the path of electrons by changing the magnetic field configuration. Thus flat profile can be easily obtained.

2.2 DESIGN AND DEVELOPMENT

The concept of hollow feeding of primary ionizing electron is schematically illustrated in Fig. 2.1-b and that of ordinary feed in Fig. 2.1-a. In these figures, the cross-sectional views of the intermediate electrode throat are shown together with magnetic lines of force. In a system that comprises the coaxially shaped magnetic nozzle like shown in Fig. 2.1-b, primary electrons accelerated through the nozzle will move along the spreading magnetic lines of force and produce a source plasma of large area.

The coaxial intermediate electrode has a center pole in an intermediate electrode chamber. The first coaxial model was prepared for the 10 cm diam. duoPIGatron ion source, where the center pole was made of an

iron rod and was equipped with a coil at the atmospheric end. The model had generated a source plasma of a very flat profile. But its density was very low due to a difficulty of getting sufficient arc discharge current. The discharge was considered to be interrupted by the leakage magnetic field in the cathode plasma and throat region.

In order to examine the magnetic structure in more detail, numerical calculations were performed with the magnetostatic computer code "TRIM"[5]. One of the results is shown in Fig. 2.2, where the ordinate corresponds to the axis of rotational symmetry and the abscissa to the radius. Thin curves denote the magnetic lines of force. This figure indicates that the source failed to form the magnetic nozzle, i.e. there is no point where the radial component of the magnetic field becomes zero in the nozzle throat between the intermediate electrode and the center pole. In Fig. 2.3, the radial component of the magnetic field is plotted at the nozzle throat (z=0.9 cm), and in the intermediate electrode chamber (z=4.4 cm), where z denotes the distance measured from the bottom of the intermediate electrode and R that from the axis of symmetry. This result shows that there is considerably strong leakage magnetic field not only in the nozzle throat but also in the cathode plasma region.

This leakage field arises from the following causes: (1) The magnetic field leaks into the chamber from the upper surface of the intermediate electrode. (2) The center pole can not completely hold the magnetic flux from the top end to the bottom end. (3) "Bridge" of the magnetic flux is apt to be formed at the nozzle throat, if there is a small imbalance of the flux density between the center pole and the intermediate electrode. These aspects were also confirmed by measurements of the magnetic field.

In order to create a field free region effectively in the intermediate electrode chamber, following reformations were made: (1) The center pole coil was exchanged for a prolonged solenoidal coil which is inserted into the intermediate electrode chamber. (2) An iron ring was installed on the top end of the intermediate electrode. (3) The gap of the nozzle throat was widened. After these reformations, the magnetic configuration has been changed to that shown in Figs. 2.4 and 2.5. This result gives nearly zero magnetic field in the cathode plasma region. Figure 2.5 shows the radial component of the magnetic field, where notations are the same as those given in Fig. 2.3. From the figure it is seen that the magnetic field intensity reaches as high as 200 gauss in

the nozzle throat region. However, this field intensity is not harmful, since the radial component of the magnetic field becomes zero at about a half way to the gap, i.e. the magnetic nozzle like that shown in Fig. 2.1-b is formed. Thus a high current arc discharge is expected in the case of Fig. 2.4. Having determined the magnetic configuration, it becomes possible to arrange the non-magnetic components such as anode and PIG-chamber. The contours of these components are added to Fig. 2.4, where magnetic perturbation caused by the cusp-magnets is ignored. In this configuration, the extraction electrode area is completely covered by the spreading magnetic flux lines that constitute the coaxial magnetic nozzle, and hence by the primary electrons which will move along the magnetic lines of force. Therefore a source plasma with a high density and a flat profile is expected to be produced.

To examine the controlling mechanism of the coaxial magnetic nozzle, the shape of the nozzle throat was changed by cutting the center pole by 2 cm as shown in Fig. 2.6. While the overall shape of the magnetic flux lines in Fig. 2.6 shows no difference from that in Fig. 2.4, the nozzle throat moves toward the axis of symmetry. Since the primary electrons will flow and enhance ionization of neutrals along the flux lines that compose the nozzle, it is expected that the density profile would be flatter in the case of Fig. 2.4 than in the case of Fig. 2.6. The iron region does not saturate for up to 5000 ampere-turns of the source coil current.

2.3 EXPERIMENTAL

The coaxial duoPIGatron ion source actually made and tested is illustrated in Fig. 2.7. Its design is based on the numerical result given in Fig. 2.4. The source is provided with a magnetic center pole in addition to the intermediate electrode, four filament cathodes, the PIG-chamber and the target cathode which a conventional duoPIGatron has. The magnetic center pole consists of an iron rod with a solenoid coil, which is surrounded by a copper water jacket for cooling. The diameter of the anode was determined in such a way that the inner surface lies just outside of the magnetic flux line which originates from the coaxial magnetic nozzle. The PIG-chamber is made of a stainless steel cylinder of 26 cm diam. around which 24 pole line cusp magnets are attached.

The PIG-chamber is referred to as the second anode, since it is electrically connected to the anode which is called as the first anode. The electrical connections are the same as those of a conventional duoPIGation. The magnetic center pole is connected to the intermediate electrode.

As the conventional duoPIGatron, the present source generates a cathode plasma and a source plasma (PIG plasma) mutually separated by the coaxial magnetic nozzle. The primary electrons produced in the cathode plasma are fed into the magnetic nozzle where they are accelerated and spread along the divergent magnetic lines of force. The source plasma is generated by these primary electrons and is confined by both the source and the line cusp magnetic field.

2.4 RESULTS AND DISCUSSION

Figure 2.8 shows the axial component of the magnetic field at 5 cm from the nozzle (Z=-5 cm) in the PIG chamber. The open circles denote the experimental results and the solid line the calculated values. They agree very well.

The density profiles of the source plasma are shown in Fig. 2.9, where the results labeled by A and B corresponds to the case of Figs. 2.4 and 2.6, respectively. The ion density was determined from the ion saturation current measured by a Langmuir probe located at about 0.7 cm above the target cathode. The case A gives a very flat profile, whereas the case B a peaked profile. These results indicate that the nozzle with larger diameter produces more flat density distribution. This is qualitatively in accordance with the numerical results described in section 2.2, and is attributable to the difference of the discharge paths due to change of the magnetic nozzle diameter and of the position of the double sheath from which electrons are emitted. A uniform density profile was obtained easily.

When the current ratio of the center pole to the source coil was constant, the profiles of the density were found to be insensitive to the currents. This result indicates that the path of arc discharge does not depend on the magnetic field intensity. This is consistent with the numerical result that the magnetic field is linear to the coil currents and hence the position of the magnetic nozzle and the shape of the

magnetic flux lines are insensitive to them.

The profile was also insensitive to the ratio of the center pole coil current to the source coil current. The numerical results show that the diameter of the magnetic nozzle decreases with the ratio of the currents, which is very similar to the case when the length of the center pole was changed. Therefore it can be said that the profile was insensitive to a small change of the center-pole length. Hereafter the results are reffered only to the case of Fig. 2.4.

In order to obtain the density profile in a plane nearer to the nozzle, the first anode was removed, and the source was operated with the second anode (the PIG-chamber) only. In this case the distance from the probe to the nozzle was shortened by 4 cm, and the target cathode moved to the position illustrated by the dotted line in Fig. 2.4. The density indicated "M" shaped profile as shown in Fig. 2.10, when the source coil current was high (above 40 A) and the discharge was not very strong (below 300 A). This result suggests that the plasma production rate is larger in the region near the wall and that the plasma diffuses from outside toward the axis of symmetry.

From these considerations it can be said that the primary electrons were fed widely into the PIG-chamber along the nozzle forming magnetic lines of force which spreads widely in the chamber. It becomes also clear that for a given grid diameter there is a optimum combination of the nozzle shape (or the center-pole length) and the height. That is, if the nozzle is located lower than the optimum the profile would be either peaked or concave. If the nozzle is located too high a uniform profile would be obtained with lower production efficiency.

2.5 FURTHER ENLARGEMENT

Preliminary results on the density distribution were described in the previous section. On the basis of the discharge mechanism of the present source, further enlargement of the plasma volume and hence the extraction area can be made easily. An example of a magnified ion source design is shown in Fig. 2.11. The size and position of the intermediate electrode and the source coil are unchanged from the previous case, while the diameter of the nozzle annulus is increased. The nozzle forming magnetic flux lines and hence the arc discharge path spread more widely

in the PIG-chamber as shown in Fig. 2.11. Thus it is expected that a source plasma with large size, and flat profile would be created by a small modification of the center pole and the intermediate electrode.

2.6 CONCLUSION

The coaxial duoPIGatron ion source has been proposed and designed. This ion source has a magnetic center pole in the intermediate electrode chamber, thereby feeding ionizing electrons widely to the PIG chamber.

Numerical calculations have been performed on the magnetic field structure for several shapes of the coaxial intermediate electrode. The source was designed and constructed on the basis of the numerical results, and was tested.

The source produced a dense plasma, whose density distribution changed in accordance with the magnetic field configuration.

It was confirmed that the primary electrons were fed widely to the PIG chamber along the widely spreading magnetic lines of force. Thus the concept of hollow feeding of electrons has proved its applicability to an ion source with large extraction area.

References

1) W.L. Stirling, C.C. Tsai, H.H. Haselton, D.E. Schechter, J.H. Whealton, W.K. Dagenhart, R.C. Davis, W.L. Gardner, J. Kim, M. Menon, and P.M. Ryan, Rev. Sci. Instrum. 50(5), 523, (1979)
2) Y. Okumura, et al., Rev. Sci. Instrum. 52(1), 1, (1981)
3) C.C. Tsai, W.L. Stirling, and P.M. Ryan, Rev. Sci. Instrum. 48(6), 651, (1977)
4) Y. Arakawa, M. Akiba, U. Kondoh, S. Matsuda, and T. Ohga, Japan Atomic Energy Research Institute Report, JAERI-M 8088, Feb., (1979)
5) J.S. Colonias, Lawrence Berkeley Lab. Report, UCRL-18439, Aug., (1968)

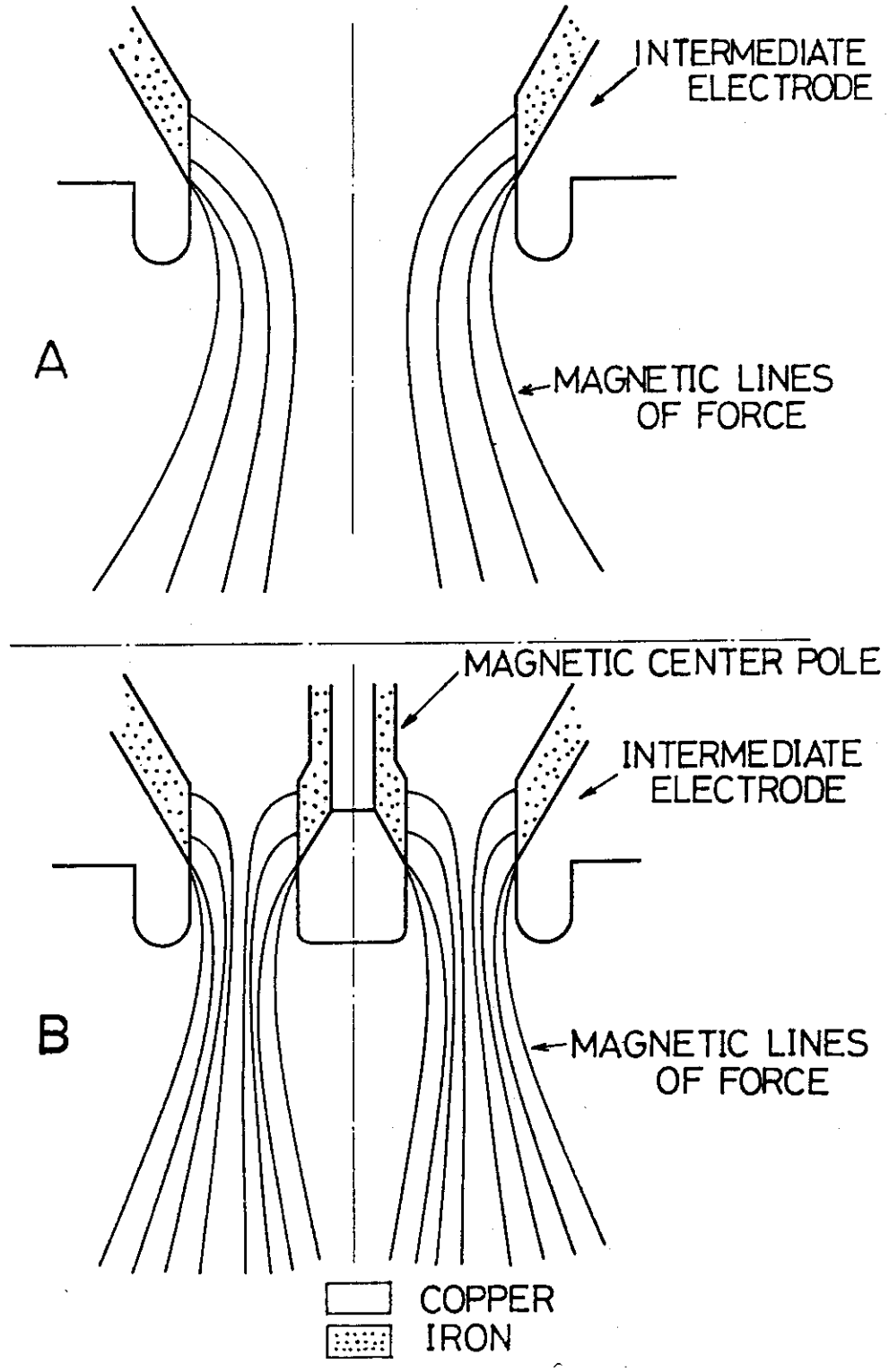

Fig. 2.1 Illustrations of cross-sectional view of the nozzle and magnetic lines of force of conventional (a) and coaxial (b) duoPIGatron.

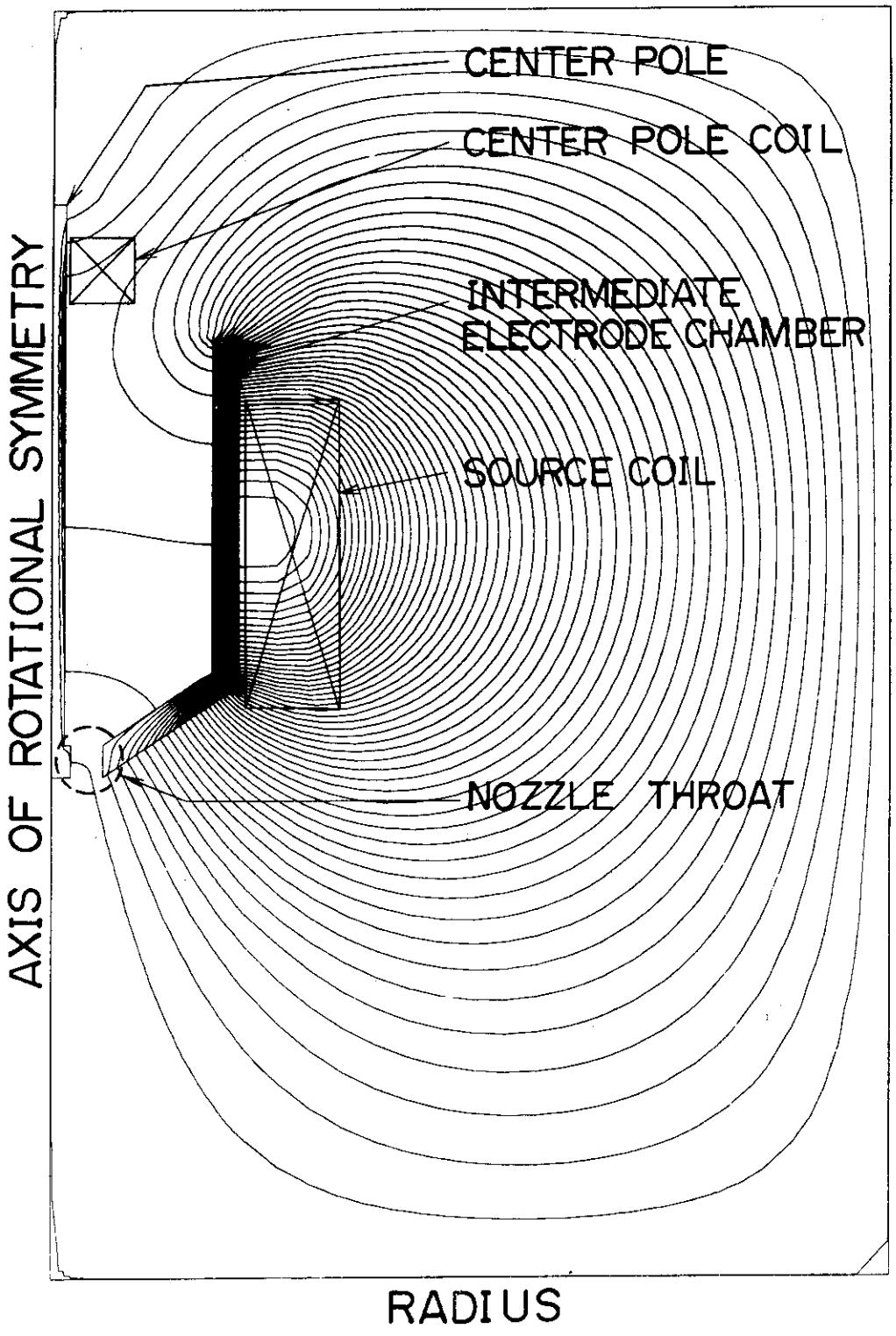

Fig. 2.2 Magnetic field structure of the first model of the coaxial duoPIGatron. The magnetomotive force of the source coil is 2000 AT and that of the center pole coil is 200 AT.

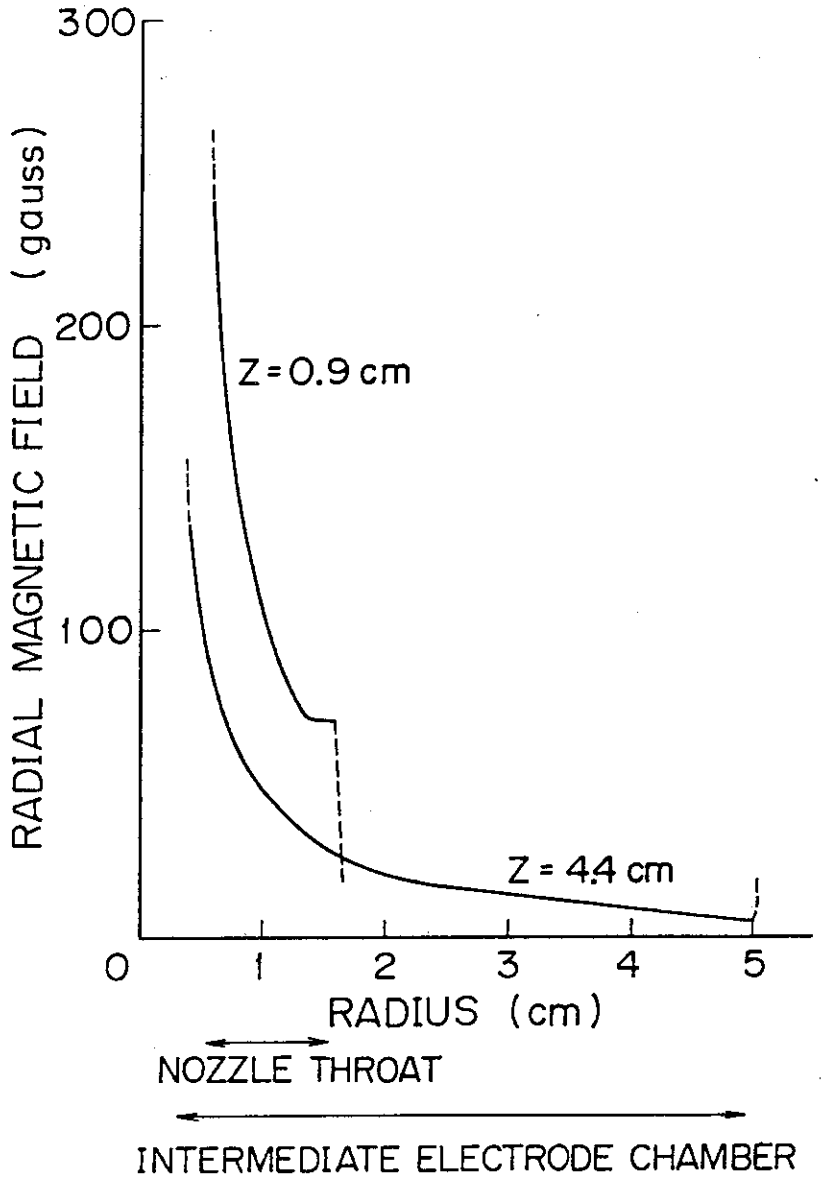

Fig. 2.3 Radial component of the magnetic field intensity in the nozzle and in the intermediate electrode chamber.

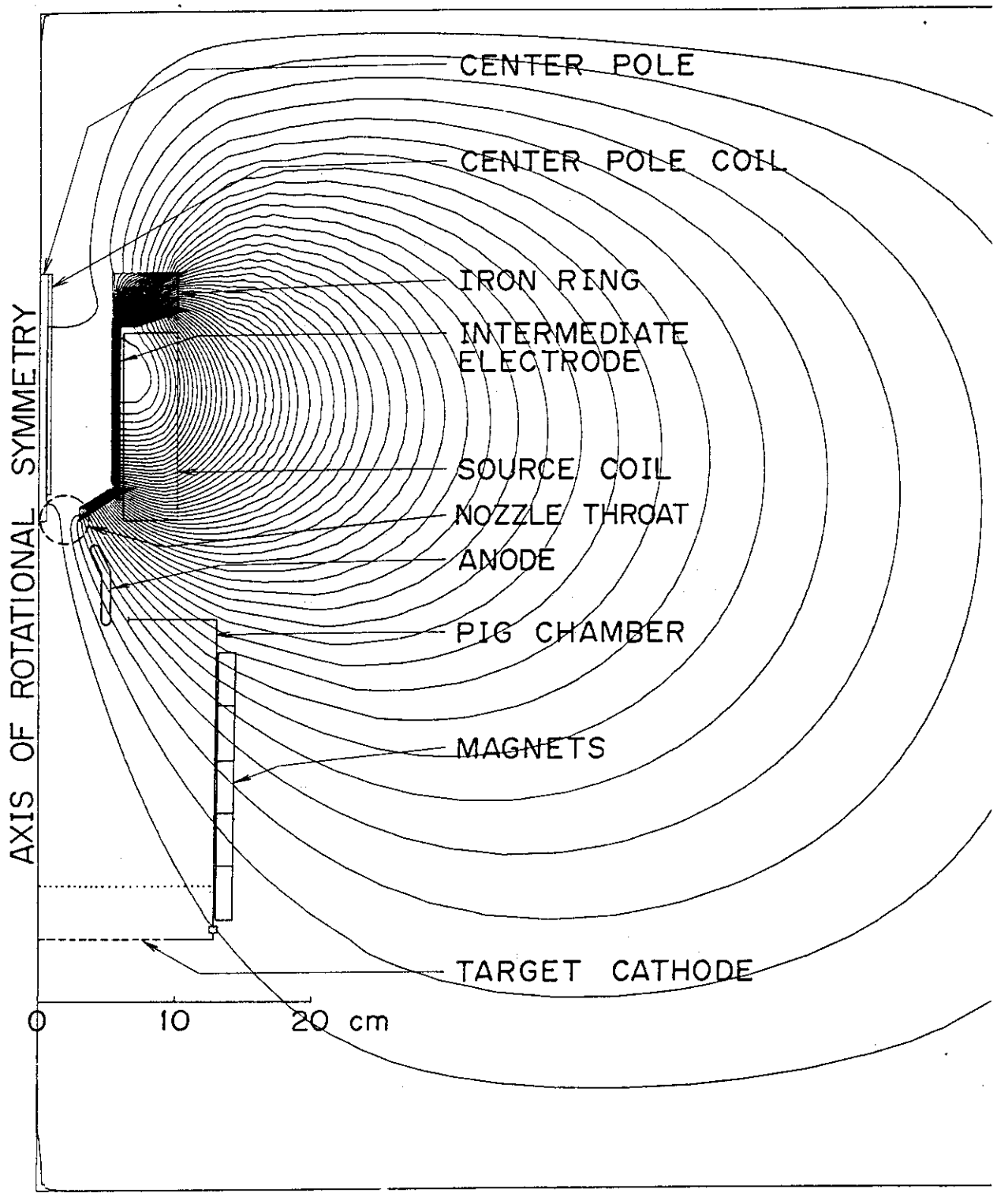

Fig. 2.4 Magnetic field structure of the optimized coaxial duoPIGatron. The main components such as anode and PIG chamber are also shown. The magnetomotive force of the source coil is 2000 AT and that of the centerpole coil is 100 AT.

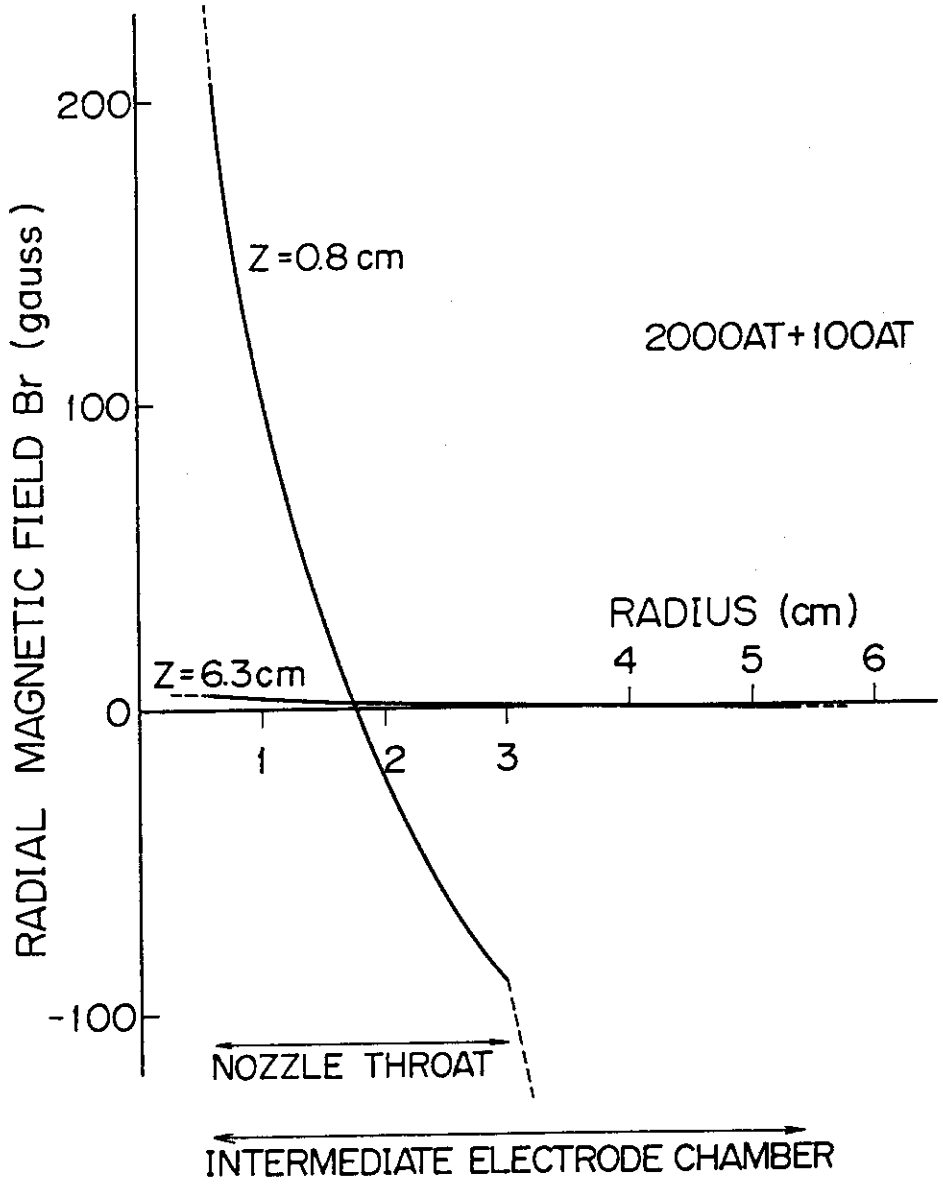

Fig. 2.5 Radial component of the magnetic field in the nozzle and in the intermediate electrode chamber in the case of Fig. 4.

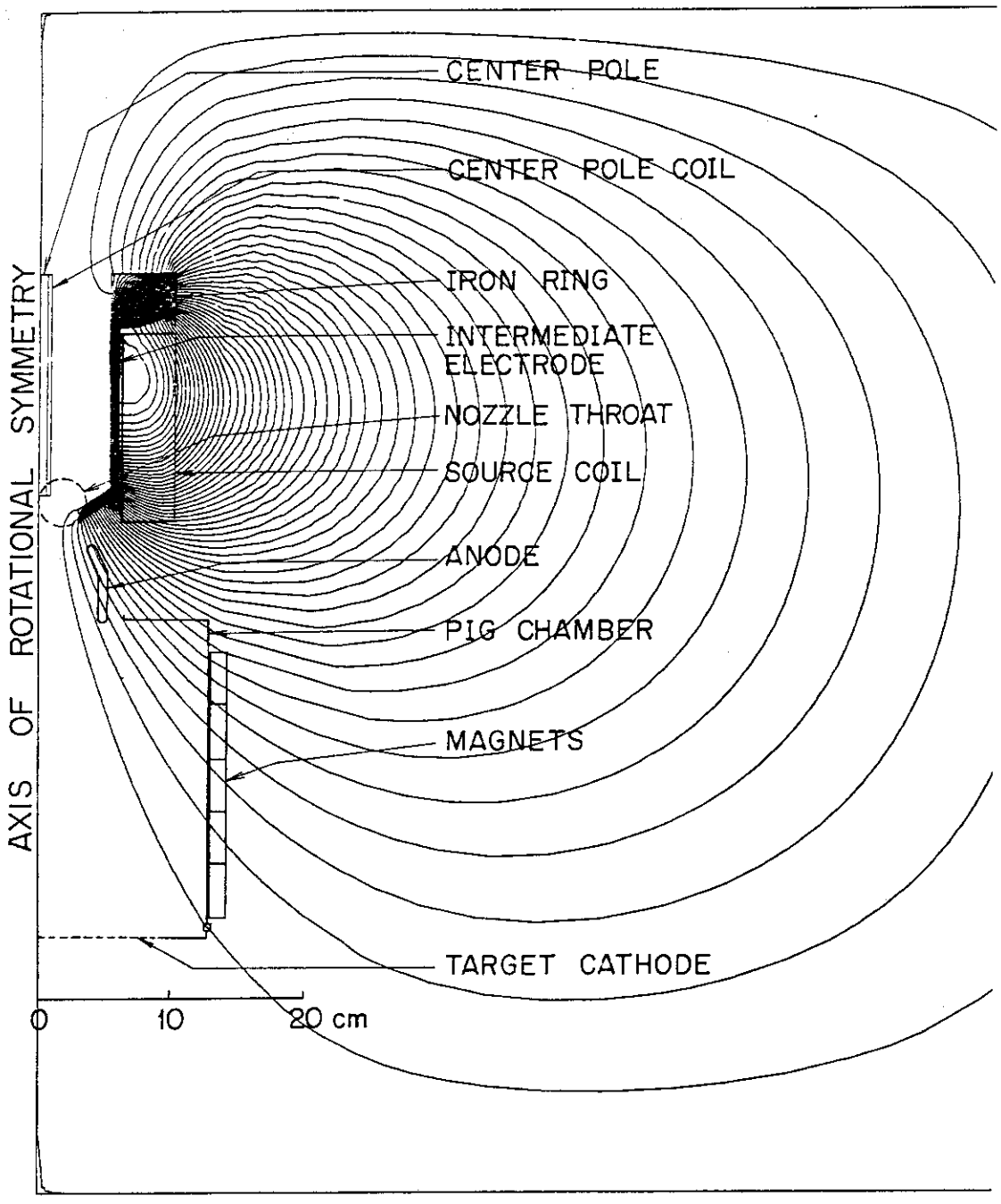

Fig. 2.6 Magnetic field structure of the coaxial duoPIGatron, when the center pole is shortened by 2 cm.

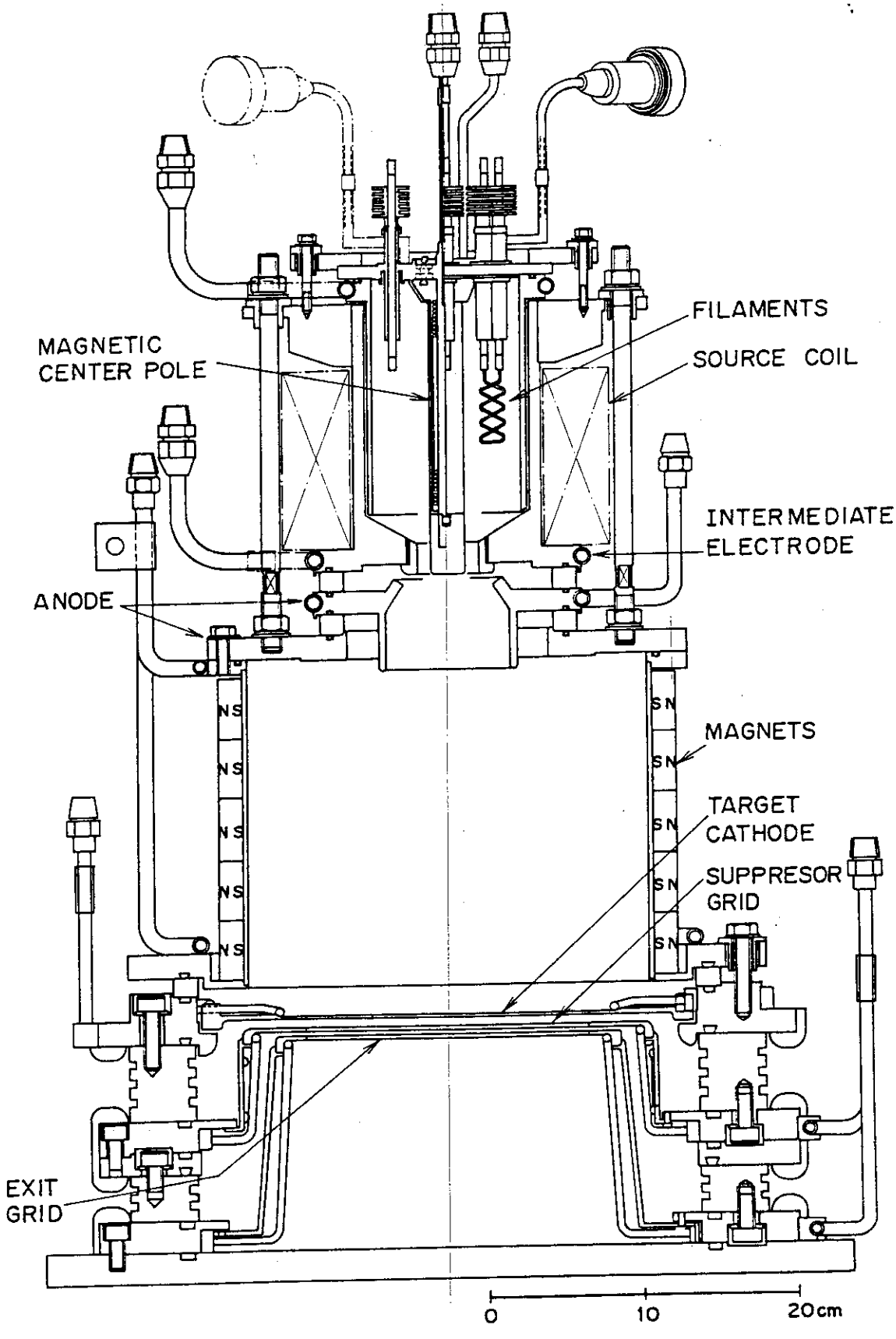

Fig.2.7 An illustration of the coaxial duoPIGatron.

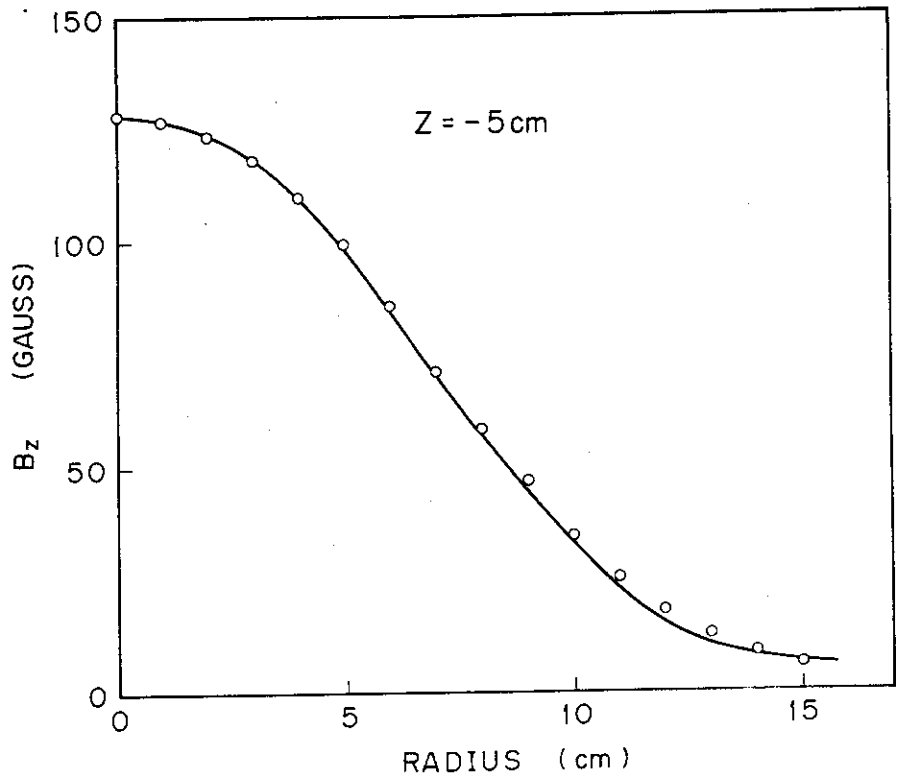

Fig. 2.8 Axial component of the applied magnetic field at 5 cm from the intermediate electrode in the PIG chamber. The magneto-motive force of the source coil is 2000 AT and that of the center pole 200 AT.

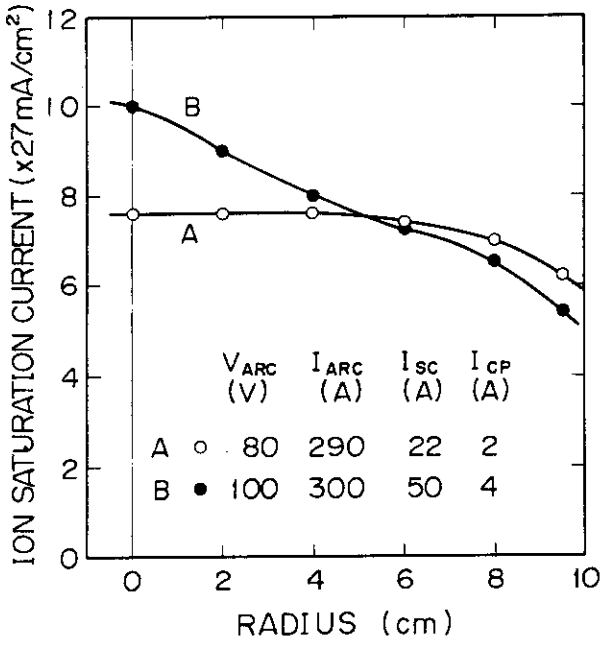

Fig. 2.9 Typical density profiles of the coaxial duoPIGatron. A and B correspond to the case of Figs.2.4 and 2.6 respectively.

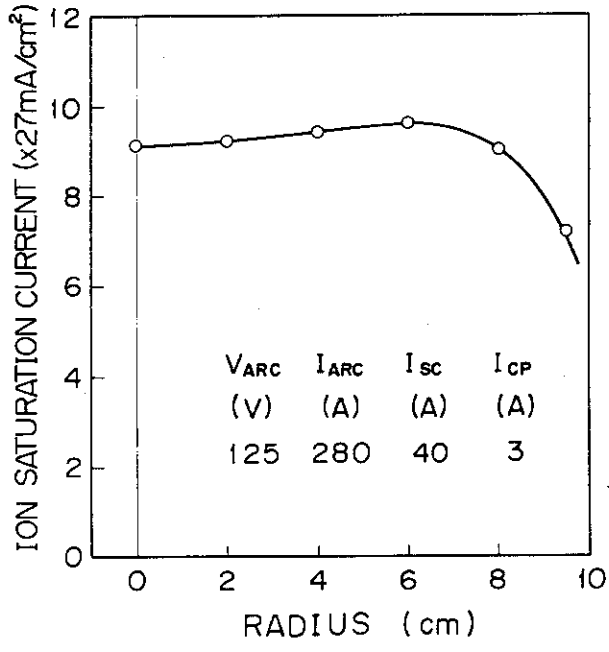

Fig. 2.10 The density profile where the first anode is removed.

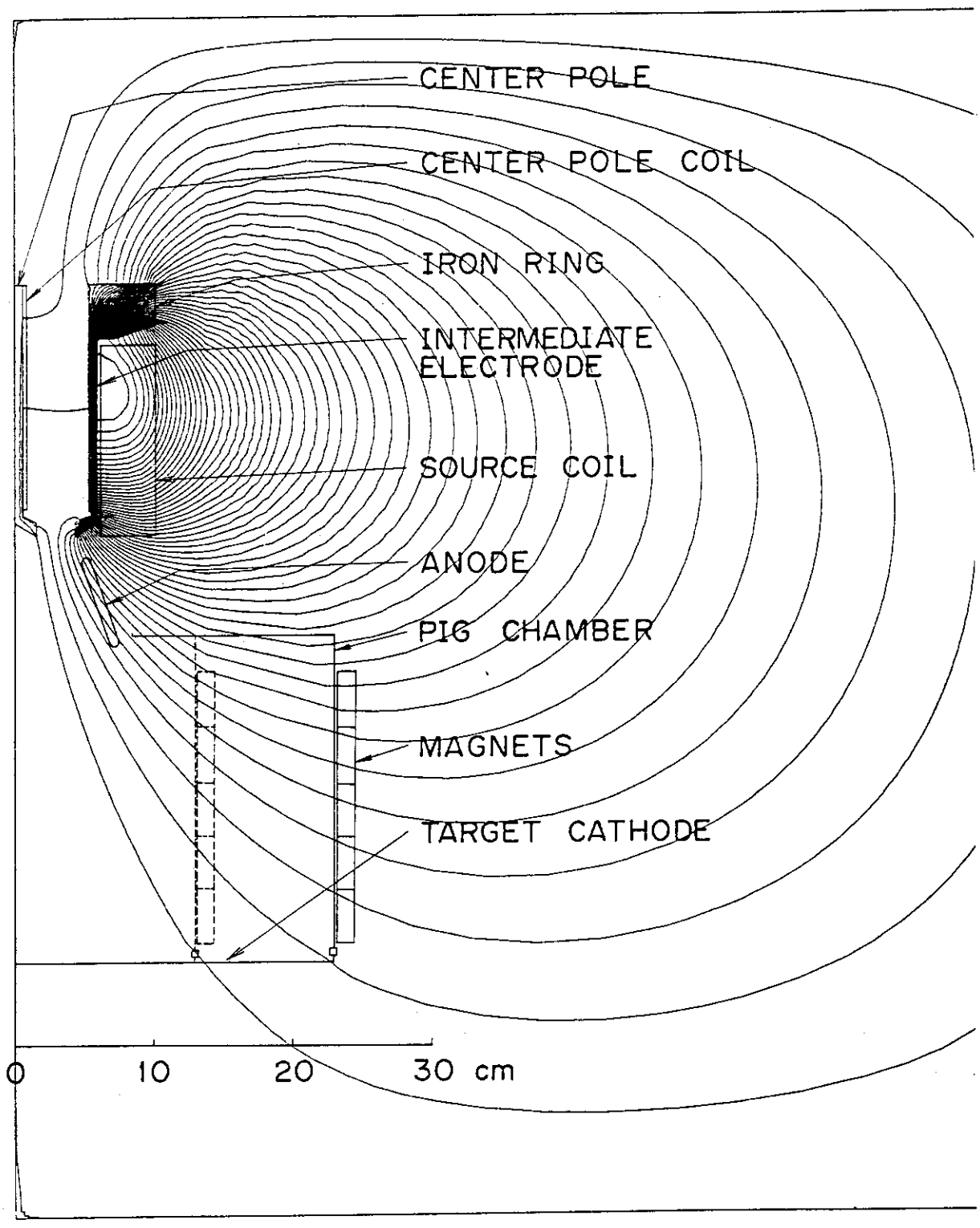

Fig.2.11 A plan of larger coaxial duoPIGatron ion source.

3.1 INTRODUCTION

The duoPIGatron ion source is one of the candidates for high current neutral beam injectors. However, its source plasma generally shows a peaked profile, when the magnetic field formed by the source coil is raised to increase plasma density. Hence it is very difficult to produce a high current beam without modification of the density distribution. One way to flatten the profile is to insert an axial button in the center of the discharge region. This approach has been pursued originally at ORNL[1] and later at JAERI[2]. The source thus developed was named as modified duoPIGatron. However, such a button tends to destabilize the arc discharge if the applied magnetic field is increased.

To produce a uniform and stable source plasma with intense magnetic field, we have proposed a new variation of the duoPIGatron ion source. The source is equipped with a coaxially shaped intermediate electrode and is called the coaxial duoPIGatron ion source. The source was designed and developed on the basis of the numerical calculation of the magnetic field, and it was confirmed that primary electrons were fed widely to the PIG-chamber along the spreading magnetic lines of force and they produce a uniform source plasma with high density.

Since there is no obstacles in the path of primary electrons, the source can be stably operated at strong magnetic field with high arc efficiency. In the present chapter, we report the effects of the applied magnetic field upon the density profile, discharge characteristics, arc efficiency and ion species. In addition, we describe the typical operation parameters and compare these with other sources.

3.2 EXPERIMENTAL

A distinctive feature of the coaxial duoPIGatron ion source is the coaxially shaped nozzle made of a magnetic center pole and an intermediate electrode. Magnetic lines of force which originate from the intermediate electrode and the center pole compose a coaxial magnetic nozzle which works as compressor and controller of the arc discharge. The whole structure of the ion source was determined as shown in Fig. 2.7 taking into account the magnetic field pattern which was obtained by numerical calculation.

The source consists of four oxide-coated filament cathodes, intermediate electrode, magnetic center pole, anode, PIG-chamber and target cathode. The magnetic center pole is made up of an iron rod of 12 mm diam with a long solenoidal coil, and is contained in a copper water jacket of 22 mm diam. An annular orifice is attached to the nozzle throat so as to mechanically adjust the throat shape and gas conductance.

The PIG-chamber is made of a stainless-steel cylinder of 26 cm diam. around which 24 column of permanent magnets are attached to form magnetic multipole line-cusp field. The magnetic field strength at the wall surface is about 1 kG, decreasing exponentially towards the axis of the chamber, and at 4 cm apart from the wall the field strength decreases to about 20 G. We employ the accel-decel three grids system with ion extracting area of 18.5 cm diam. and the beam transparency of 49 %. Hydrogen gas is introduced into the intermediate electrode chamber through a pulsed valve just before the arc voltage is switched on. A pulsed arc voltage is applied between the anode and cathode. The PIG-chamber is directly connected to the anode. The coaxial intermediate electrode and the target cathode are returned to the arc supply positive terminal through resisters of 1 kΩ and 200 Ω, respectively. Thus, these electrodes are essentially kept floating.

3.3 RESULTS AND DISCUSSION

a. Density Profile

In the coaxial duoPIGatron ion source, the primary electrons are guided along the divergent magnetic lines of force, scattered widely in the PIG-chamber and produce a uniform source plasma. The typical density distributions of the coaxial source are shown in Fig. 3.1, where V_{ARC}, I_{ARC}, I_{SC} and I_{CP} denote the arc voltage, arc current, source and center pole coil currents, respectively. The density was measured by a Langmuir probe located at about 0.7 cm above the target cathode. The spatial density variations are small over 18.5 cm diam grid, and are ±8 % and ±11% in the case of open and solid circles, respectively. The density is sufficiently high and uniform for the production of high current ion beam.

The profile was insensitive to the applied magnetic field, which

indicates that the discharge path does not change with the field intensity. This fact shows a clear contrast with the conventional duoPIGatron case where the profile is very sensitive to the applied magnetic field strength.

b. Discharge Characteristics

The arc voltage changes depending on the arc current and on the two coil currents. The relation between the discharge voltage and the center pole coil current is indicated in Figs. 3.2 and 3.3. It is seen from Fig. 3.2 that the arc voltage shows minimum at 2 A of the center pole coil current. This voltage gradually increases with the arc current as shown in Fig. 3.3, which is generally observed in the conventional duoPIGatron sources. The arc voltage seems to become insensitive to the center pole coil current with an increase of the arc current.

The relation between the plasma density and the center pole coil current is shown in Figs. 3.4 and 3.5 where the ordinates denote the density measured at the center of the chamber. The density suddenly increases when the center pole coil current is increased from 1 to 2 A, corresponding to the dip in the arc voltage shown in Fig. 3.2. However, further increase of the center pole coil current above 2 A is ineffective since the increasing rate of the density with the current is smaller than that of the arc voltage, i.e. the arc efficiency is highest at 2A (the arc efficiency is defined by the ratio of the extracted beam current to the arc power).

The increase of the arc voltage above 3 A of the center pole coil current is traced to the leakage field in the cathode plasma region, generated as a result of imbalance of the flux density between the intermediate electrode wall and the center pole. This can be supported by the results of numerical calculation of the magnetic field discussed in chap. 2. The leakage fields increase the arc impedance, thereby increase the arc voltage.

The arc voltage always showed minimum and the density suddenly increased when the center pole coil current was raised to 1/10 of the source coil current, and then the operation of the source was most stable. Thus it is verified that the coaxial magnetic nozzle is well formed at a ratio of the two coil currents of 1/10. Comparing the case where the source coil current is 30 A, shown in Fig. 3.5 with the 20 A case in

Fig. 3.4, we find that the density becomes more sensitive to the center pole coil current with an increase of the source coil current. However, above 1/10 of the cource coil current, the density becomes insensitive to the center pole coil current so that the adjustment of the current is not critical. Hereafter the results are referred only to the case when the center pole coil current is adjusted to be 1/10 of the source coil current.

c. Arc Efficiency

The source plasma density increases with the arc voltage, arc current and applied magnetic field intensity. An increase of the magnetic field raises the density since it increases the arc efficiency and the discharge voltage. Comparing the open and solid circle cases in Fig. 3.5 shows that the efficiency rises by about 6 % with increasing the source coil current from 20 to 30 A for a constant gas flow rate. While the efficiency was further increased, the source plasma became unstable when the current was raised to 50 A.

The arc efficiency became highest when the gas flow rate was reduced to near the lower limit of stable discharge region. And it reached 1.5 and 1.3 A/kW for the source coil current of 30 and 20 A, respectively, at the ion saturation current density of 250 mA/cm^2. However in the case of modified duoPIGatron, the efficiency is limited to 1.1[3] or 1.2[4] A/kW for the equal beam transparency. This is because an increase of the magnetic field destabilizes the arc discharge in the case of the axial button and impairs the uniformity in the case of no button.

The open circles and squares in Fig. 3.5 correspond to the results when the height of the coaxial intermediate electrode was changed by 3.5 cm. The arc efficiency of the open circle case becomes higher by 10 to 15 % than that of the square case. This increase results from the decrease of loss area of the line cusp, since magnetic insulation of the anode and the coaxial intermediate electrode is considered to be nearly constant.

These results indicate that the arc efficiency is sensitive not only to the applied magnetic field intensity but also to the effective line cusp area. Thus the efficiency may be further increased if the height of the coaxial intermediate electrode from the target cathode is lowered through the design of a more divergent magnetic field structure.

d. Ion species

A high ratio of proton yield is desired to increase penetration of neutral beam into the torus plasma. To achieve higher proton ratio it is important to produce a source plasma of higher electron density with better particle confinement[5]. This is because the dissociation of molecular ions is enhanced with the electron density, and the recombination of protons to molecules can be reduced by improving the particle confinement. In Fig. 3.6 is shown the ion species fraction as a function of the applied magnetic field, where the ion beam current ranges from 15 A to 20 A. This figure shows that the proton ratio increases monotonically with the applied magnetic field, since the density becomes high and the confinement better with the field intensity. The operation with high magnetic field is therefore desirable for the efficient production of ion beams with high proton ratio.

The proton ratio is improved to 70 % from 60 % of the modified duoPIGatron for JFT-2 neutral beam injector[4] which possesses the same PIG-chamber with the same magnetic line cusp field as those of the present source. This proton ratio is still lower than the reported data of the PLT source[3], probably due to smaller volume of the source plasma.

3.4 TYPICAL OPERATION PARAMETERS

The present source generated a dense and uniform plasma over the grid of 18.5 cm diam., and produced ion beams of 30 A at 30 kV which were limited by the capacity of the high voltage power supply of the test stand. Typical operating parameters are listed in Table 3.1. The source was stably operated at the source coil current of from 20 to 40 A, and was most stable at 30 A.

From the viewpoint of cathode reliability, the coaxial duoPIGatron as well as the non-coaxial duoPIGatron have advantages over the magnetic multipole ion source[4] of smaller number of breakdown in the arc discharge, smaller damage of the cathode and lower impurity concentration in the beam[6], which are attributable to the isolated cathode from the main plasma.

3.5 CONCLUSION

The coaxial duoPIGatron ion source has been built and tested. The source generated a dense and uniform source plasma over the grid of 18.5 cm diam., and produced ion beams of 30 A at 30 kV which were limited by the capacity of the high voltage power supply of the test stand. Typical operation parameters are listed in Table 3.1. The density profile of the source plasma was not affected by an increase of applied magnetic field intensity, which shows a clear contrast with a conventional duo-PIGatron case. The coaxial intermediate electrode worked well at a fixed ratio between the center pole coil current and source coil current, indicating that the magnetic nozzle has successfully connected the cathode with source plasma region. The arc efficiency was found to be sensitive to the effective area of the line cusp magnetic field, and to the applied magnetic field. The efficiency defined by the ratio of the extracted beam current to the arc power reached 1.5 A/kW at the source coil current of 30 A, when the operation of the source was most stable. The ion species fraction was measured and the proton ratio was increased to 70 % from 60 % of the modified duoPIGatron. The applied magnetic field was also effective for the production of ion beams with high proton fraction.

References

1) W.L. Stirling, C.C. Tsai and P.M. Ryan, Rev. of Sci. Instrum. 48(5), 533, (1977)
2) Y. Arakawa, M. Akiba, U. Kondoh, S. Matsuda and T. Ohga, Japan Atomic Energy Research Institute Report, JAERI-M 8088, Feb. (1979)
3) W.L. Stirling, C.C. Tsai, H.H. Haselton, D.E. Schechter, J.H. Whealton, W.K. Dagenhart, R.C. Davis, W.L. Gardner, J. Kim, M.M. Menon and P.M. Ryan, Rev. Sci. Instrum. 50(5), 523, (1979)
4) Y. Arakawa, et al., Japan Atomic Energy Research Institute Report, JAERI-M 8869, May (1980)
5) S. Tanaka and T. Shibata, Japan Atomic Energy Research Institute Report, JAERI-M 7966, Nov. (1978) (in Japanese)
6) Y. Okumura, Y. Mizutani, Y. Ohara and T. Shibata, Rev. Sci. Instrum. 52(1), 1, (1981)

Table 3.1 Typical operation parameters of the coaxial duoPIGatron ion source.

Accel Voltage	30 kV
Extracted Current	30 A
Arc Voltage	75 V
Arc Current	330 A
Source Coil Current	20 A
Center Pole Coil Current	2 A
Gas Flow Rate	9.5 Torr·ℓ/sec
Pulse Length	100 m·sec

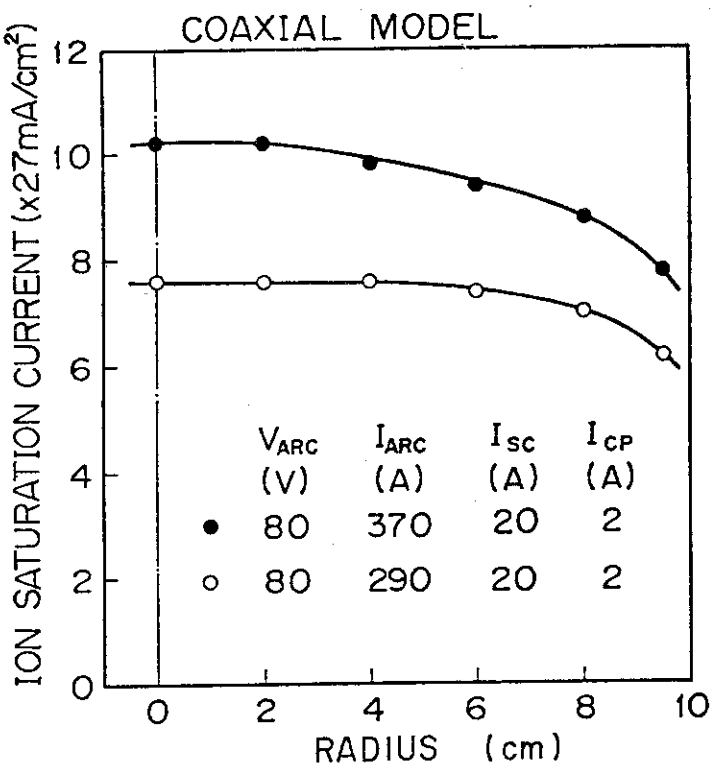

Fig. 3.1 Typical density profiles of the source plasma of the coaxial duoPIGatron.

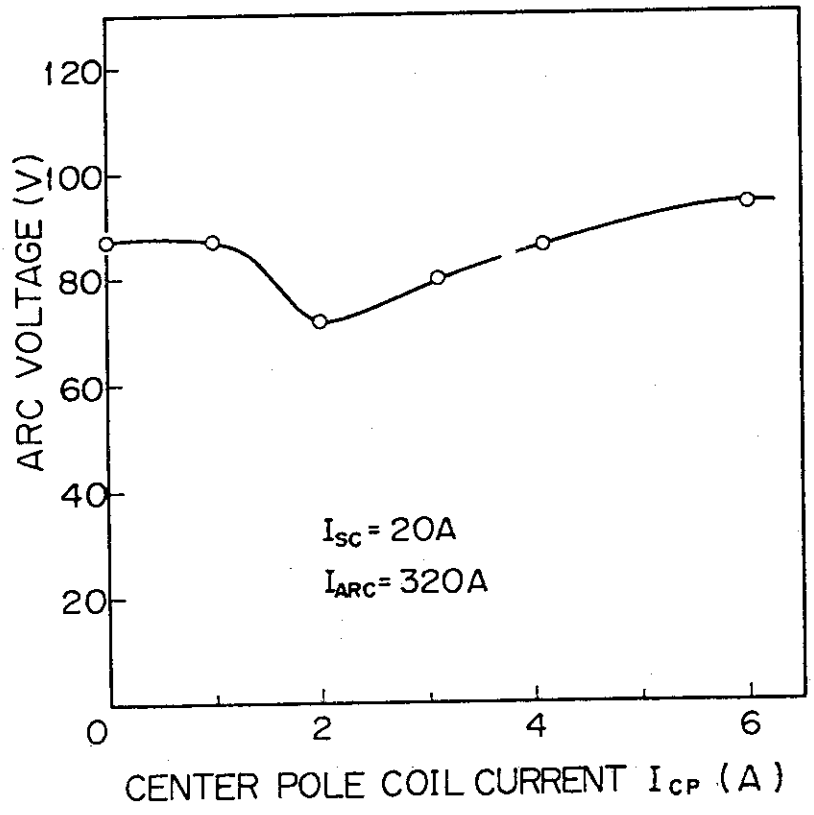

Fig. 3.2 Arc voltage as a function of the center pole coil current.

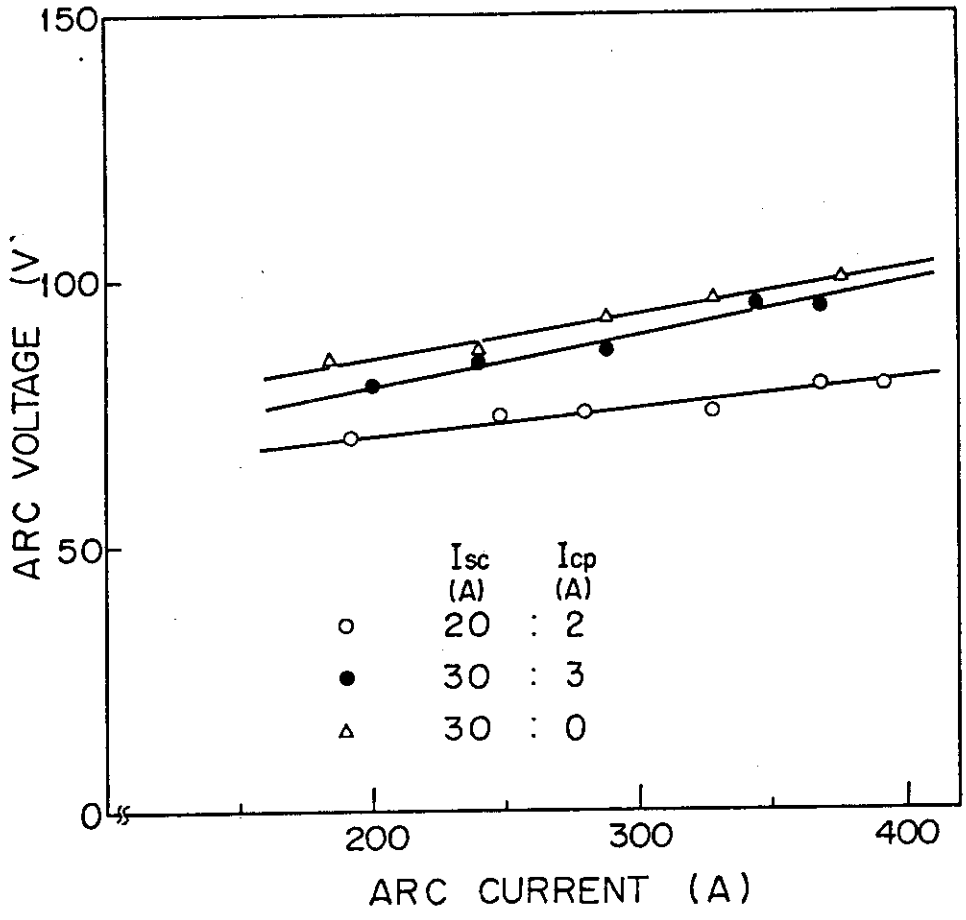

Fig. 3.3 Relation of the arc voltage to the arc current.

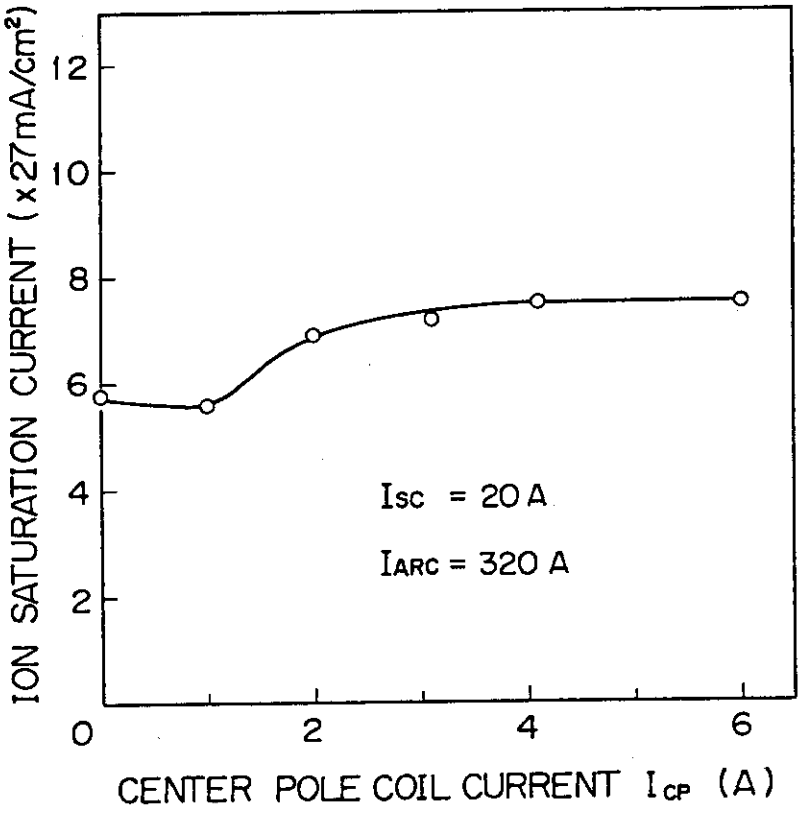

Fig. 3.4 Plasma density as a function of the center pole coil current. The plasma density was measured at the center of the chamber.

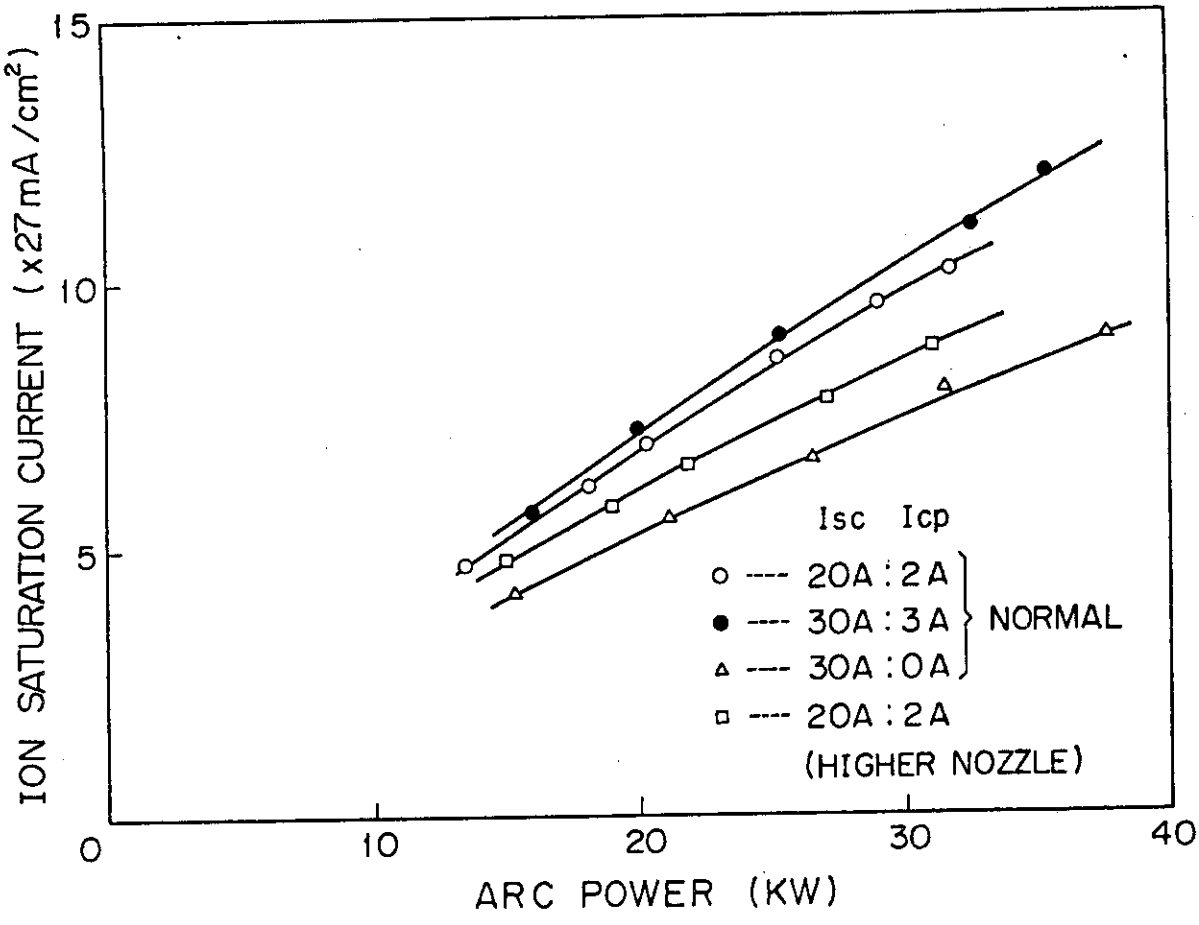

Fig. 3.5 Plasma density as a function of the arc power. The plasma density was measured at the center of the chamber.

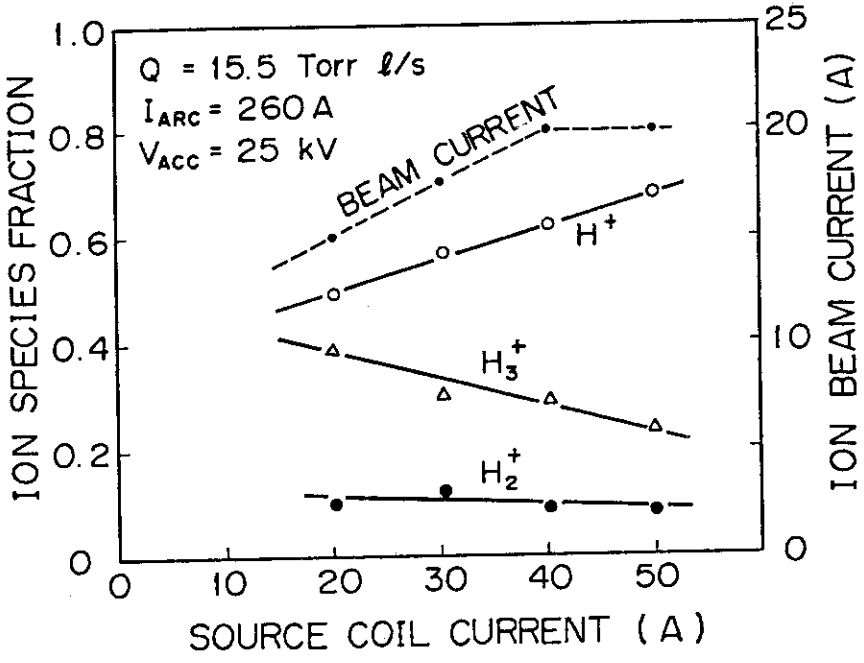

Fig. 3.6 Ion species fraction as a function of the applied magnetic field strength, when the center pole coil current is adjusted to be 1/10 of the source coil current.

4.1 INTRODUCTION

Intense ion sources are being developed to produce quasi-continuous megawatt neutral beam. For instance the ion source for JT-60 neutral beam injection is specified to deliver an ion beam of 35 A at 75 keV for up to 10 s[1]. Each extraction electrode is equipped with alternately arranged rows of apertures and water cooling pipes over the 12 cm × 27 cm area, which determines a beam transparency of 40 %.

In these ion sources, heat loading to the extraction electrode is one of the crucial problems which limit the ion beam power density. Measurements of the heat loading to a two-stage extraction system showed that up to 2 % of the extracted beam power was dissipated in an electrode under the typical beam divergence and gas pressure[2]. The corresponding heat loading averaged over the cooling surface is 270 W/cm^2. This heat loading may cause thermal deformation or melting of the electrode during a pulse of 10 s. due to its small heat capacity.

It is well-known that there are two methods of removing the heat from the electrodes. One of the methods is the heat removal by coolant and the other is the radiation cooling. In order to test the radiation cooling method, graphite electrodes were employed. However, the extraction of ion beams was frequently interrupted by electric breakdowns between electrodes and many hydrocarbon ions were contained in the beam[3]. The graphite electrodes appear to be inadequate for the ion source of NBI.

Thus active cooling is necessary for the long-pulse operation. Requirements for the cooling system of the electrode are as follows: Do not reduce the electric breakdown limit between the grids, and do not disturb the electric field near the apertures and hence the ion beam trajectories. To satisfy these requirements, the cooling system consists of many small cooling channels connected in parallel. In the parallel cooling channels flow distribution is not very stable. A decrease of flow rate in a channel may cause a hot region leading to distortion of the grid matrix.

Up to now, several experiments on the cooling of the extraction electrodes have been conducted by H.C. Cole[4], L.D. Stewart[5] and R. Becherer[6]. They carried out the experiments with a short pulse length and with a small ratio of power loading to heat capacity of the electrode. In this chapter, we report the experiments on the cooling of

the electrodes with forced water for a longer pulse length of up to 10 seconds, and a target that simulated an electrode which extracts a megawatt of ion beams.

4.2 EXPERIMENTAL

The experiment was performed by using a 10 cm diam. duoPIGatron ion source[7]. This ion source had the singe stage accel-decel extraction system, whose electrodes were made of oxygen-free copper. The grid was a disk of 10 cm in diam. and 2.0 mm in thickness, through which 284 beam apertures of 3.75 mm in diam. were drilled. On the surface of each grid, sixteen copper pipes of 1.8 mm in outer diam. and 0.3 mm in thickness were silver-soldered. Row of apertures and the cooling pipes were alternately arranged as shown in Fig. 4.1 and the beam transparency was approximately 40 %. The temperature of the ground electrode was measured by chromel-alumel thermocouples which were buried at the center and at the supporting flange of the electrode (see Fig. 4.1). The thermocouples were electrically insulated from the surrounding stainless steel sheath of 0.5 mm in diameter.

The experimental set up is illustrated in Fig. 4.3, where the target was set 70 cm apart from the extraction electrode of the ion source. The target was a copper disk of 18 cm in diam. and 5 mm in thickness. Eighteen parallel cooling tubes, 2.5 mm in outer diam and 0.5 mm in thickness were silver brazed in such a way that they were wholly buried in the rear side of the target. The disk temperature was measured with chromel-alumel thermocouples buried at various positions indicated by filled circles in Fig. 4.2.

The experiment was carried under the condition that the ion beams of 1 to 5 A at 30 keV were extracted for 0.1 to 10 sec. Flow rate of the cooling water for the electrodes was 1 to 3 ℓ/min. and the coolant pressure ranged from 0.6 to 1.2 MPa.

The flow rate of cooling water for the target was set constant at 10 ℓ/min. Water pressures at the inlet and outlet of the target were 0.7 MPa and 0.67 MPa, respectively.

4.3 EXPERIMENTAL RESULTS AND DISCUSSION

a. Power loading to the electrodes

The ions being accelerated in the extraction region collide with the background gas and give rise to degraded energy particles, H_2^+ ions and H^0 neutrals, and to electrons. Some of these particles can strike the electrodes creating a power loading problem. The contributing factors to electrode loading may be listed as follows (Fig. 4.4):

(1) Direct interception of electrode by ions on high aberrated trajectories. These ions give rise to secondary electrons which carry energy back to the positive grid or to the source.

(2) Slow ions produced by charge exchange and ionization of the background gas. Some of these ions strike electrodes producing secondary electrons which deposit energy on the plasma grid or on the source.

(3) Electrons produced by ionization. Some of these electrons also strike the positive grid.

(4) Ions from the neutralizer. Beam plasma is generated in the neutralizer. Beam plasma ions are extracted by the negative potential of the deceleration electrode and give rise to secondary emission of electrons. Some of them strike either the positive or ground electrode.

(5) Heating of the positive grid by the source plasma. These power loadings are almost proportional to neutral pressure and sensitive to the beam divergence and to the cross-sectional shapes of the grid apertures. The beam divergence is affected by the gap lengths between the electrodes. The ratio of the dissipated power in electrodes to the extracted beam power increases with the beam divergence, for the direct interception of ions by grids increases in accordance with the beam divergence.

The heat dissipation rate can be reduced below 2 % of the total beam power by chamfering the extraction holes and/or by proper choise of the gap length. However, in this experiment the grids with the straight holes were employed and the gap lengths were chosen so as to give large beam divergence and high heat fluxes to the grids. The gap lengths were set to be 5.5 mm and 3.2 mm for the acceleration and deceleration gaps, respectively. Beam divergence and power loading to each electrode were measured as a function of extraction current, as shown in Fig. 4.5. Large beam divergence and hence large power dissipation in the grids were obtained in our experiment. The loading to the positive and to the

negative electrodes increased with the extraction current as shown in Fig. 4.5, which were 2 to 3 % and 0.3 % of the total beam power, respectively. On the other hand, power loading to the ground electrode did not depend on the extraction current of 2 to 5 A which was constantly about 6 kW. This value is equivalent to the heat load of 130 W/cm^2 when averaged over the copper grid area*. The load on the ground grid indicates that the ratio of the power loading to the ion beam power decreases with an increase of the ion current. This is attributable to decrease of beam divergence, and to change of the beam profile which is thinner than the Gaussian profile at lower current than the optimum value and fatter at higher current than the optimum. Hereafter the results are referred only to the ground electrode since it suffered the highest power loading of the three electrodes.

b. Measurement of temperature of the ground electrode

In the case of short pulse

Figure 4.6 shows an example of the time dependence of temperature rise at the center of the ground electrode in the case of pulse length of 1 sec. As expected, the temperature rose after the beam initiation and then fell after switching off of the beam. It should be noted that in Fig. 4.6 there is a sudden fall of the temperature of about 10 °C with the characteristic time constant of about 10 msec just after the termination of the beam. In order to interpret the sudden fall, we drew a dotted line as shown in Fig. 4.6. Characteristic time of heat conduction in a material is given by

$$\tau = d_c^2/(4a) \quad , \tag{1}$$

where d_c is the characteristic length of heat conduction and a is the diffusion coefficient of temperature in the material. The relation between the heat flux q and the temperature difference ΔT is given by

$$q = \lambda \Delta T/d_c \quad , \tag{2}$$

where λ is the thermal conductivity of the material. Substituting d_c = 2.45 mm, which is the distance between the thermocouple and the wall

---

* $6000/(1-0.4)5^2\pi = 130$ W/cm^2

of the cooling pipe, and assuming a heat source of 20 W on the mid plane between pipes, which is equivalent to power loading per aperture of the ground electrode (6 kW/284 apertures), we then estimate the time constant and the temperature difference from eqs. (1) and (2) to be 13 msec and 14 °C, respectively. In addition to the above estimation, heat conduction around an aperture part was numerically calculated by means of a computer program for two-dimensional non-steady heat conduction on the assumption that there was a heat source of 20 W around the inner surface of each aperture. The result showed that the time constant and the temperature difference were 12 msec and 12 °C, respectively. Consequently, the difference between the solid line and the dotted line in Fig. 4.6 is attributed to the temperature difference between the point of thermocouple and the wall of cooling pipe.

In Fig. 4.6, there is another interesting time behavior of the temperature. After the sudden fall discussed above, the temperature falls exponentially with the time constant of order of one second. This decay line for 0.6 sec after the sudden fall, however, shows a slight convex difference from the ideal exponential decay curve. This is attributed to the heat flow from the supporting flange of the electrode, which has a larger heat capacity, to the measuring point.

From many other measurements we can evaluate the time constant for cooling the electrode. Figure 4.7 shows the time constant as a function of the flow rate of cooling water. As expected the time constant decreases with the flow rate.

In the case of long pulse

Experiments with the pulse length of up to 10 sec were extensively performed. An example of temperature rise at the center of the electrode is shown in Fig. 4.8, when the ion beams of 1.3 A at 30 keV was extracted for 9.4 s and the total flow rate of cooling water was 2 ℓ./min. Figure 4.9 shows the time response of temperature rise at the center (1) and at the edge of the supporting flange (2) when the ion beam of 3.8 A at 30 keV was extracted for 7.3 s with cooling water flow rate of 2.8 ℓ./min. The temperature at the center rose to saturate within a few seconds after the beam initiation and then fluctuation of the temperature was observed. The equilibrium temperatures were about 200 °C and 230 °C in the case of Fig. 4.8 and Fig. 4.9, respectively. From the fluctuation of the temperature and the equilibrium temperatures, it can be recognized

that the nucleate boiling had occurred in the pipes.

In the subcool boiling heat fransfer, the wall superheat ΔT_{sat} is given by the empirical equation of Thom et al.[8],

$$\Delta T_{sat} = 0.0243\ q^{0.5}\ \exp(-p/88.6) \quad , \tag{3}$$

where p is the pressure of the cooling water. Assuming that the average heat flux q is 100 W/cm^2 and the water pressure is 1 MPa, we can calculate ΔT_{sat} to be 20 °C. In Fig. 4.10 the equilibrium temperature of the electrode is shown as a function of water pressure. The solid line in the figure represents the saturation temperature of water at corresponding pressure.

The difference between the experimental points and the solid line corresponds to the sum of the superheat of the wall and the temperature difference between the thermocouple and the pipe wall. The sum becomes about 30 °C using the values mentioned previously. The broken line in Fig. 4.10 which is 30 °C above the saturation temperature shows a good agreement with the experimental points. It can be understood that the temperature rise at the center of the ground electrode was suppressed by the boiling heat transfer.

The cross-sectional view of the electrode shown in Fig. 4.1 can be divided into two sections: the grid region and the flange region. Some of the heat power dissipated in the electrode were stored in the electrode and the others were carried away by the cooling water. In order to estimate these heat quantities, the time-dependent temperature distribution of the flange was calculated numerically by means of heat conduction code "TRUMP"[9], using the temperature rise of the flange edge which is shown in Fig. 4.9-2. The heat was assumed to be generated at the rate of Q(t) W/cm^3 at the edge of the grid region. We tried various forms of Q(t)'s to compare the temperature rises at the edge of the flange region (Fig. 4.11 thin lines) and the experimental result (Fig. 4.11 thick line). From this figure, it is seen that the heat generation rate is less than 380 W/cm^3 and this value corresponds to the heat inflow of 0.5 kW from the grid region to the flange region. The temperature rise at the edge of the grid region is also estimated. The result together with Fig. 4.9-2 shows that the temperature of the grid region rose by about 30 °C for the latter 4 seconds of the beam pulse. Thus the power being stored in the grid region can be estimated to be 0.4 kW. Namely, in the temperature

saturation region the power of 5.1 kW out of 6 kW was removed by water and 0.9 kW was being stored in the electrode. The former value corresponds to the heat flux of 100 W/cm^2 on the cooling surface. Since the heat of 0.9 kW being stored in the electrode was very small compared with that carried away by the coolant, the heat load at the cooling surface would increase by only 15 % even if the complete thermal equilibrium state was established.

In our long-pulse tests, the pulse length was not limited by the heat removal ability of the electrode but by the occasional electrical breakdowns between the acceleration structures or by instabilities of arc discharge.

c. Heat loading to the target

In Fig. 4.12 is shown the evolution of the temperature rise at the center of the target when it was irradiated by an ion beam of 3.8 A at 30 keV for 7.6 s. The temperature rise was saturated at about 180 °C at 0.8 s after the beam initiation. This figure also shows that all the input power after this saturation was transferred to the cooling water except for small radiated power. The incident power to the target obtained from the calorimeter was 57 kW. Thus the average heat loading to the cooling surface and to the target surface becomes 570 W/cm^2 and 220 W/cm^2, respectively. The target was bombarded more than 100 times by the ion beams ranging from 1 to 4 A at 30 keV for 1 to 7.6 s. But no sign of burnout was observed.

4.4 CONCLUSION

The experiments was made on extraction electrodes of an ion source in the case of long pulse operation. A copper electrode with forced water cooling copper pipes worked well under the condition that ion beams of 1 to 5 A at 30 keV were extracted from the source with the pulse length of 0.1 to 10 sec. In this case the heat loading averaged over the copper grid area of the ground electrode was about 130 W/cm^2 and the heat loading to the cooling surface was 100 W/cm^2.

Temperature of the ground electrode was measured by two thermocouples and was suppressed below 230 °C by the aid of nucleate boiling heat

transfer from the electrode to cooling water.

A disk target was irradiated by hydrogen beams of up to 4 A at 30 keV for 7.6 s. The average heat loading was as high as 570 W/cm^2 on the cooling surface and 220 W/cm^2 on the target surface.

In order to satisfy the requirements of the ion source for JT-60 NBI system, heat dissipation of 2 % of the total beam power must be removed from the electrode, which is equivalent to the heat flux of 270 W/cm^2. We have to handle the heat flux which is in a factor of 2 higher than that of the present experiment in the electrode. However, the heat loading to the cooling surface of the target exceeds the requirements of the ion source for JT-60. Thus the extraction grid can be designed to withstand the operation of 35 A at 75 keV for 10 s. from the heat transfer point of view.

On the other hand the average heat flux to the target surface, 220 W/cm^2 can not be justified for the design bases. It should be evaluated from the point of view of thermal deformation and fatigue, taking into account of the actual electrode geometry.

References

1) S. Matsuda, M. Akiba, Y. Arakawa, H. Horiike, T. Itoh, U. Kondoh, Y. Ohara, T. Ohga, T. Shibata, H. Shirakata, T. Sugawara and S. Tanaka : Second Large Tokamak Meeting (IAEA), Princeton, Nov. (1976).
2) Y. Okumura, Y. Ohara and T. Ohga : Japan Atomic Energy Research Institute Report, JAERI-M 7696 (1978).
3) U. Kondoh, H. Horiike, H. Morita, T. Sugawara and S. Tanaka : Japan Atomic Energy Research Institute Report, JAERI-M 7612 (1978) (in Japanese).
4) H.C. Cole, D.P. Hammond, E.M. Jones, A.C. Riviere and J. Sheffield : Culham Laboratory Report, CLM-P 313 (1973).
5) L.D. Stewart and W.L. Stirling : Proc. of the 2nd Sympo. on Ion Sources and Formation of Ion Beams, Berkeley, California, Oct. (1974).
6) R. Becherer : Proc. of the 9th Sympo. on Fusion Technology, Garmisch-Partenkirchen (FRG), June, (1976).
7) S. Matsuda, T. Itoh, U. Kondoh, Y. Ohara, T. Shibata, H. Shirakata, T. Sugawara and S. Tanaka : Japan Atomic Energy Research Institute Report, JAERI-M 6431 (1976) (in Japanese).
8) J.R.S. Thom, et al.: Proc. Inst. Mech. Engr. Pt. C 180-3 (1966).
9) L. Edwards : UCRL-14754, May (1968).

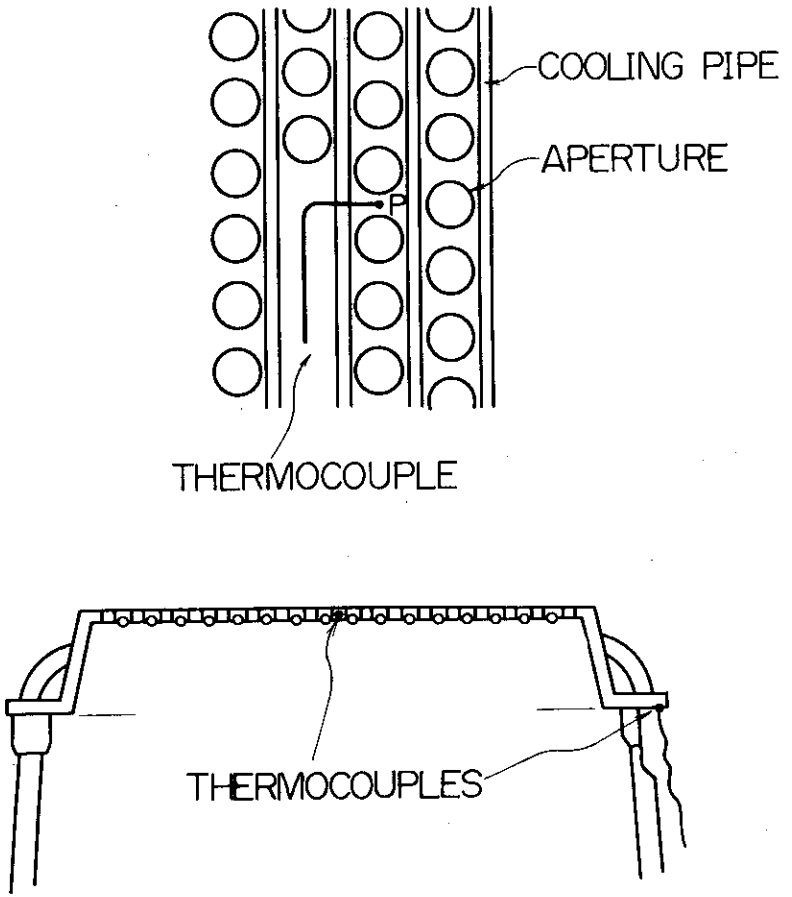

Fig.4.1 Arrangement of beam apertures and cooling tubes. The cross section and the temperature measuring points of the ground electrode are also shown.

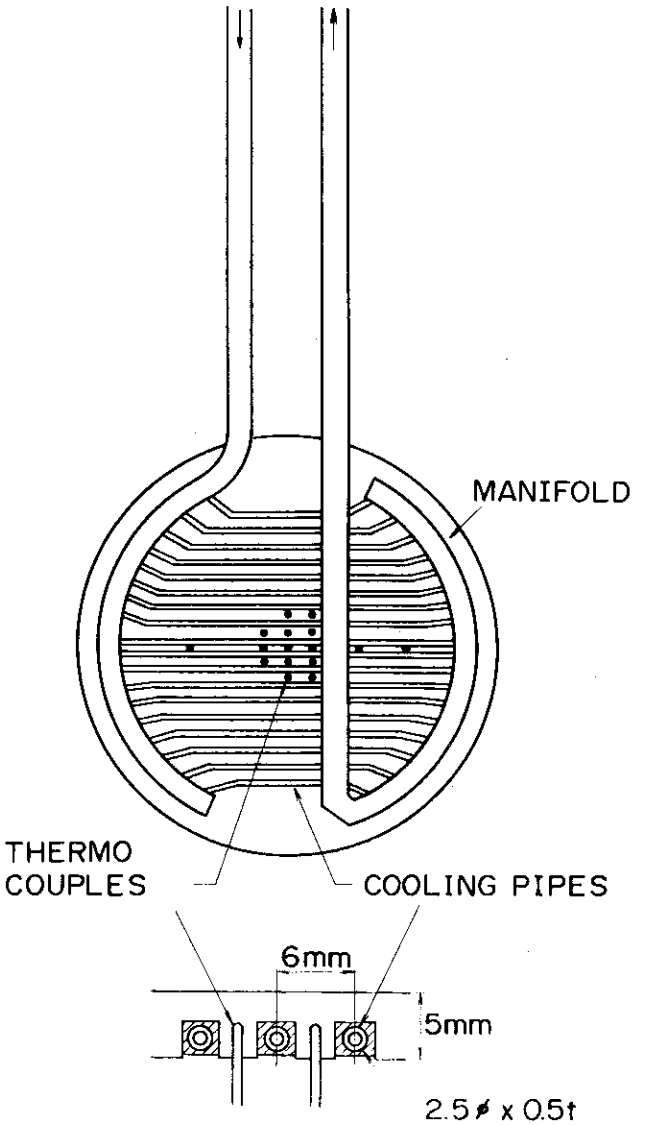

Fig.4.2 Plain view and cross sectional view of the target.

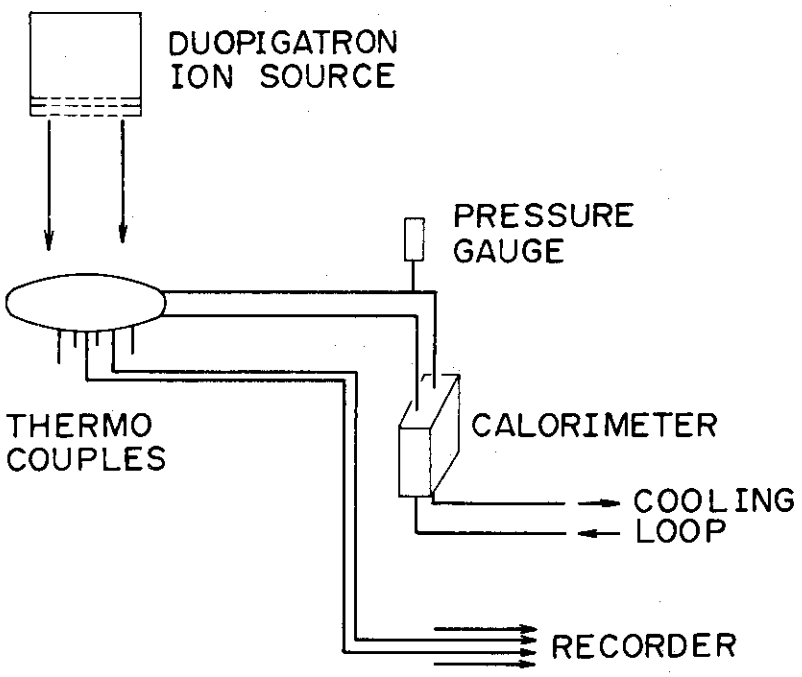

Fig.4.3 Experimental set up.

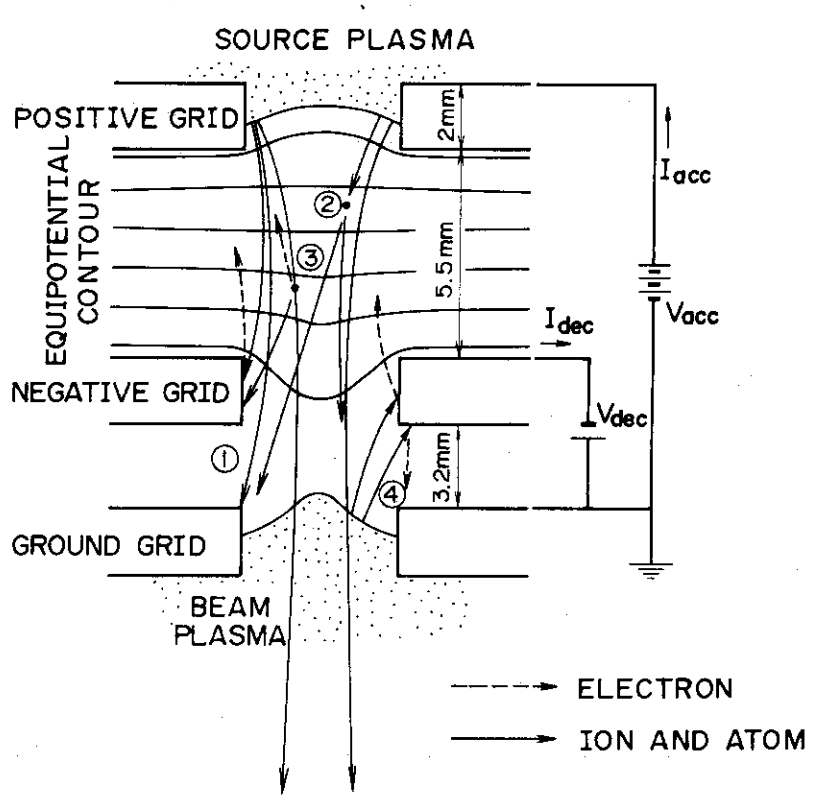

Fig.4.4 Schematic diagram of the beam extraction region.

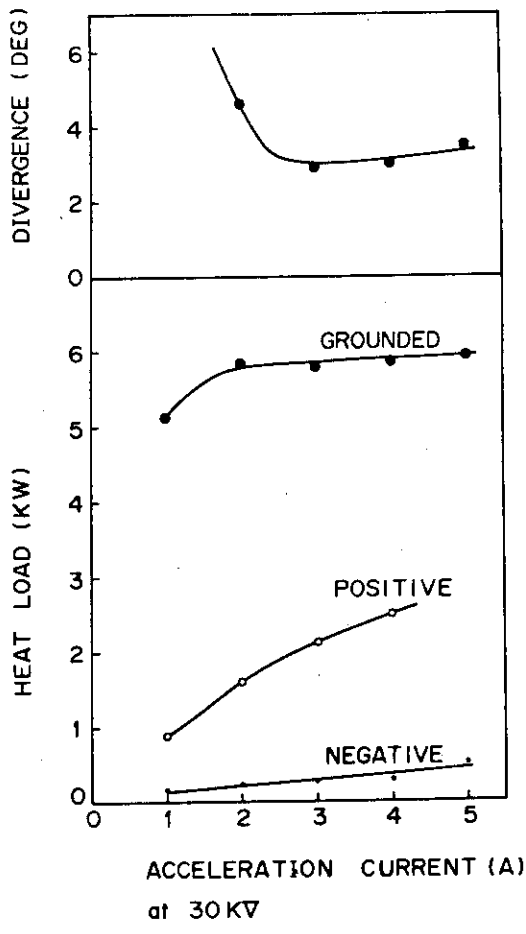

Fig. 4.5 Lower part show the heat load on the each electrodes. Upper shows the beam divergence as a function of the ion current.

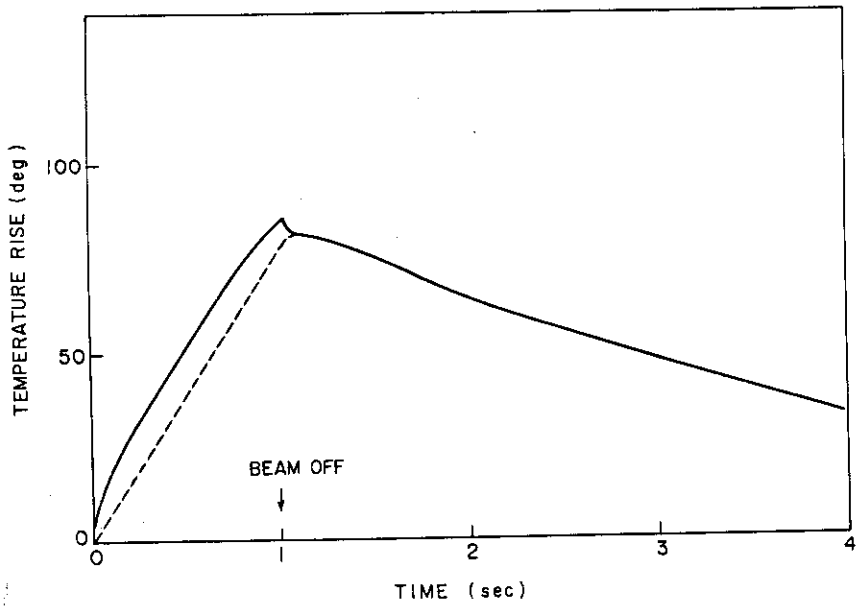

Fig. 4.6 Time evolution of the temperature rise at the center of the ground electrode, when an ion beam of 2 A at 30 keV was extracted for 1 s. Flow rate of water was 2.5 ℓ/min.

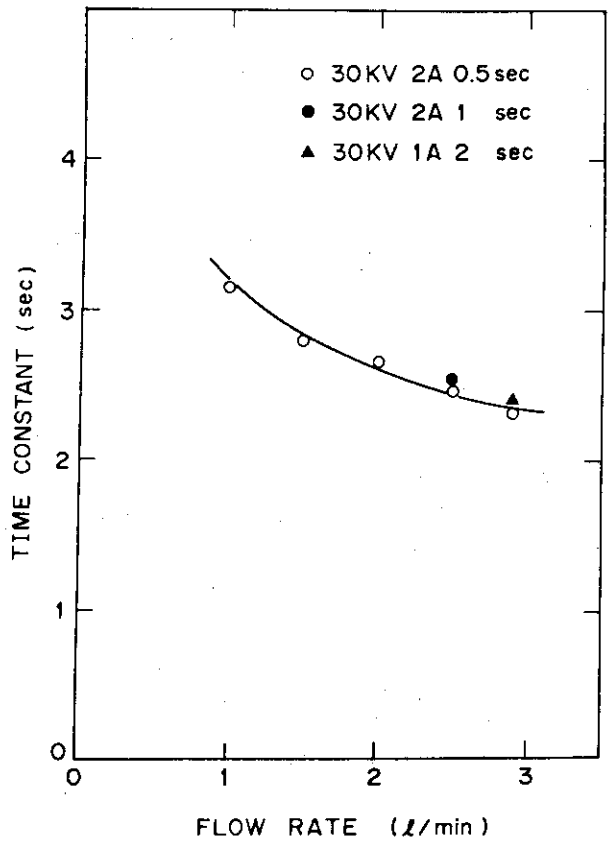

Fig. 4.7 Time constant for cooling the copper electrode as a function of flow rate of coolant water.

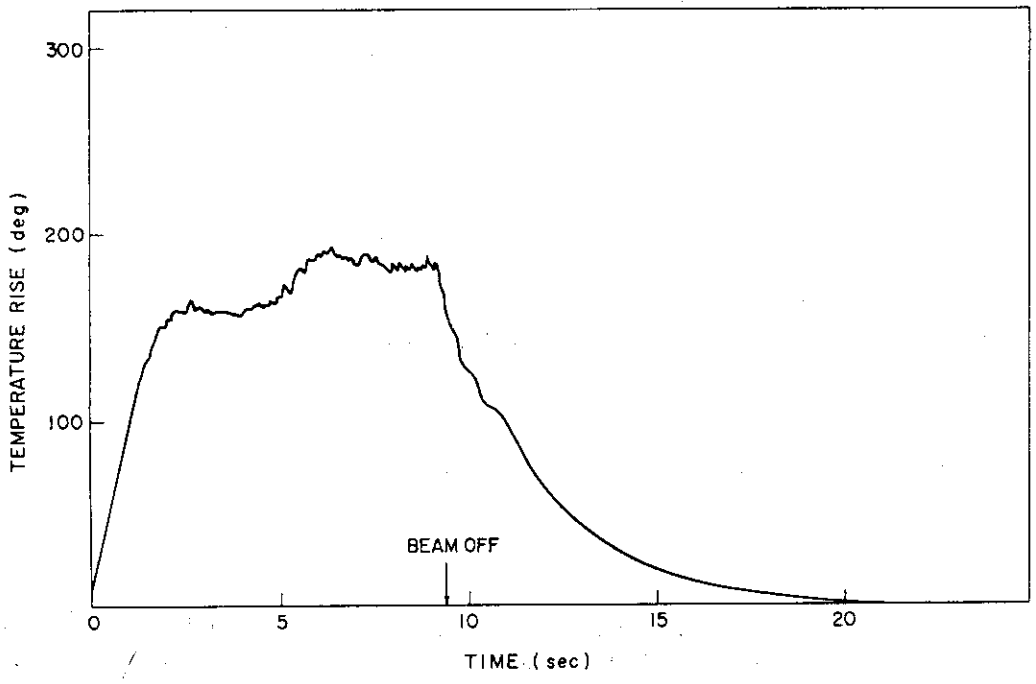

Fig. 4.8 Time evolution of the temperature rise at the center of the electrode, when an ion beam of 1.3 A at 30 keV was extracted for 9.4 s. Flow rate of water was 2 ℓ/min.

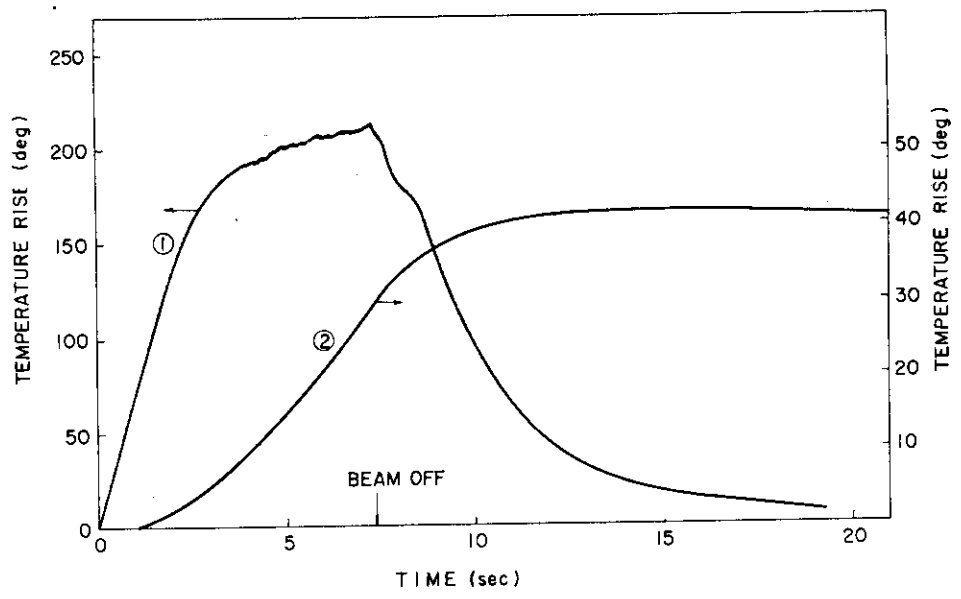

Fig. 4.9 Time evolution of temperature rise at the center (1) and at the edge of the supporting flange (2) of the electrode, when an beam of 3.8 A at 30 keV was extracted for 7.3 s. Flow rate of cooling water was 2.8 ℓ/min.

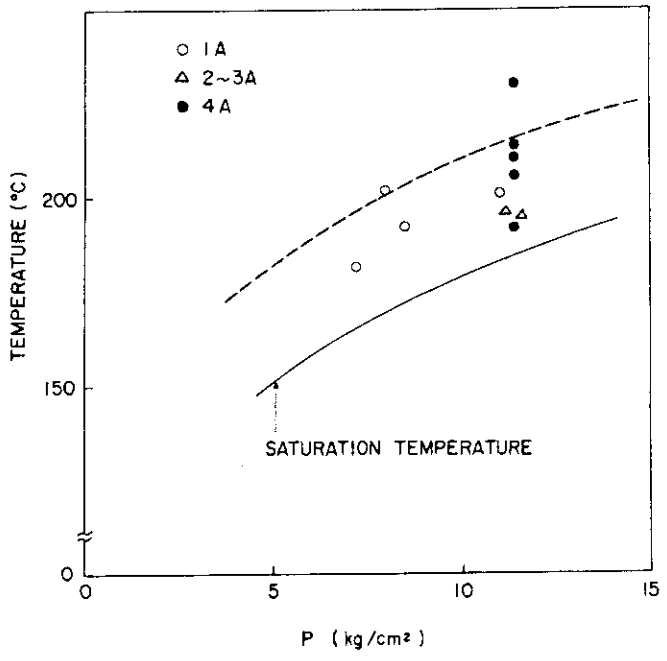

Fig. 4.10 Equilibrium temperature at the center of the electrode as a function of water pressure. Solid line represents the saturation temperature of water.

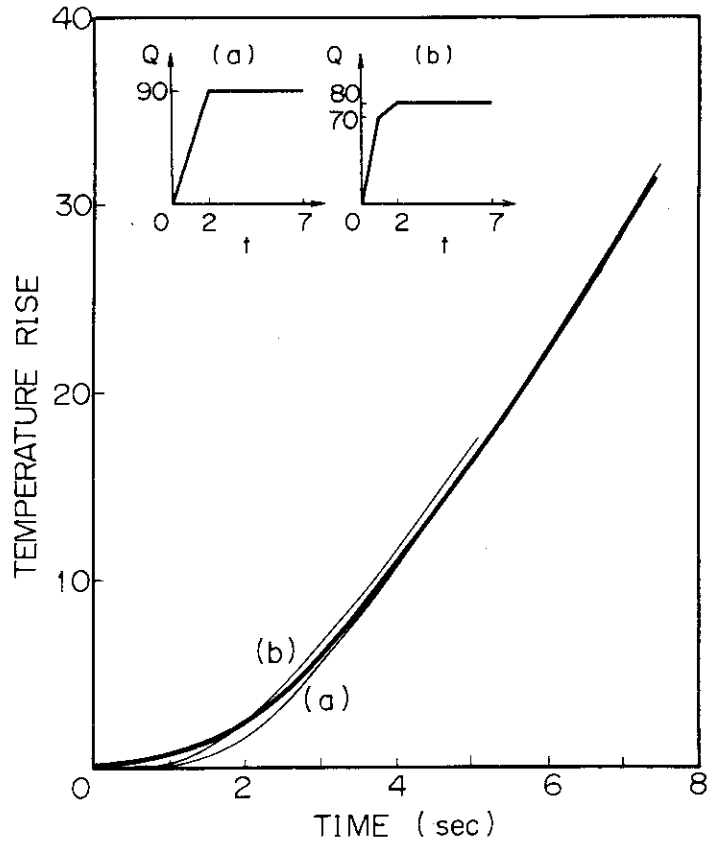

Fig. 4.11 Temperature rise rate at the edge of the flange region. The thin lines show the numerical results and the thick line the experimental result.

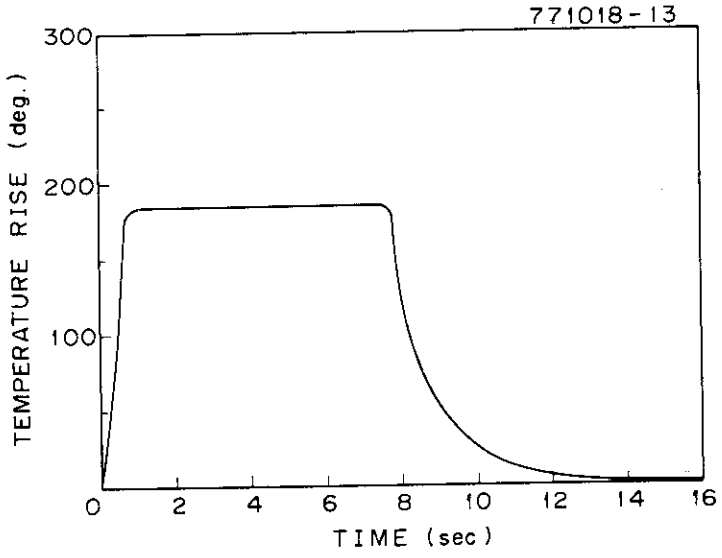

Fig. 4.12 Time evolution of the temperature at the center of the target in the case of 3.8 A at 30 keV for 7.6 s.

5.1 INTRODUCTION

Heat removal from beam dumps is one of the serious problems in the design of the high power high energy neutral beam injector for large tokamaks such as JT-60 (JT-60 NIB)[1].

For the cooling of these beam dumps two methods may be employed, since the JT-60 NBI operates in a series of pulses of 10 s with low duty cycle. One is the active cooling and the other is the passive cooling (inertial cooling). In the latter case, the heat load on the cooling surface is mitigated temporally owing to large heat capacity of thick slab. Thus burnout is improbable. Instead, thermal stress is very large, which is caused by temperature gradient across the slab. Hence it is very difficult to design a passively cooled beam dump unless heat energy deposited by a pulse is sufficiently small[5].

We have adopted the active cooling method making use of thin wall cooling tubes, which are made of the oxygen free copper with 0.2 % silver added. This material was selected because it is superior in softening temperature (350 °C), and is comparable in thermal conductivity to pure oxygen free copper. Our cooling tube is provided with fins which intercept energetic ions, leading to reduction of temperature gradient and hence thermal stress across the tube[6]. Calculation shows that the temperature of the heated surface is suppressed below 300 °C for the heat flux of 5 MW/m^2. This is very important to minimize the heat loading to cryo panels at L. He temperature.

A reliable estimate of burnout heat flux is required for the design of beam dumps which comprise thin wall cooling tubes. While many burnout data have been accumulated in subcooled forced convection systems[7),8)], most experiments have been performed under uniform heat flux distribution in both peripheral and axial directions. It is uncertain if these data can be applicable to our case, where cooling tubes of the dumps are always heated from one side with non-uniformly distributed ion beams. In addition, incident heat flux due to ion beams is independent from the wall conditions, which are different conditions from most of reported experiments in high heat flux region, where joule heating were employed as heat sources.

Therefore we have conducted burnout test of the finned tube by means of ion beam irradiation. The experiment was carried out for distilled water in a highly subcooled forced convection system, with

local heat fluxes of 8 MW/m^2 to 15 MW/m^2. The results are compared with reported burnout correlations, and yield a simple correlation.

5.2 EXPERIMENTAL

The experimental set up is shown in Fig. 5.1. The test channel was installed at the bottom of the vacuum chamber 2 m high, and the ion source at the top.

The test channel is shown in Fig. 5.2. A 1 m long tube was four folded to heat cooling water up to an appropriate subcooling temperature. It was installed with inclination at 23 °C to the beam axis for reducing the surface heat flux. The linear sections were made of finned tubes whose cross-sections were shown in Fig. 5.3. The tube material was 0.2 % silver bearing copper.

Cooling water flowing in the test channel was heated gradually by an ion beam with broad distribution, and was most intensely heated at the center of the most downstream quarter section. Thus burnout is considered to breakout at this point, where water temperature is highest and pressure lowest. The experiment was conducted with respect to this quarter section, which refers to the test section hereafter.

Surface temperature of the test section was measured with thermocouples at positions shown by solid circles in Fig. 5.2. These thermocouples were chromel-alumel type with the sheath 0.5 mm diam., and were buried with silver-brazing in grooves cut on the surface. Exit temperature of the cooling water was measured with a thermocouple inserted into the tube at 70 cm downstream from the test section. Bulk temperature at the center of the test section (burnout point), was determined from the exit temperature by use of the correlation,

$$T_b = 0.9\ (T_{OUT} - T_{IN}) + T_{IN}$$

which was obtained prior to burnout test, by using another test channel provided with both thermocouples for measuring the bulk and exit water temperatures. Pressure was measured at the inlet by a Bourdon tube, and at the outlet by a Bourdon tube and strain gage pressure transducer. Signals from the thermocouples and those from the pressure transducer were recorded by a multi-pen recorder.

Flow diagram is shown in Fig. 5.4. Distilled water was circulated in a closed loop by a pump with a maximum outlet pressure of 1 MPa. The flow rates were measured by area flow meters. The water was always refined by ion exchange resin, and was monitored by insulation resistance. The loop was made of stainless steel and teflon tube, except the pump and small parts such as the flow meter. It is therefore considered that rust and dissolved gas had a negligible effect on experimental results. The flow rate and the local pressure were controlled with two throttles at the inlet and outlet of the test channel.

Ion beams were produced by a duoPIGatron ion source with two-stage acceleration grids of 10 cm diam.[9),10)] The ion source can generate hydrogen ion beams of 5 A at 70 keV for up to 10 sec. Beam intensity profile was measured with a multichannel photo beam monitor[11)] and a movable calorimeter.

Heat flux distribution on the test channel was interpolated from the beam profiles obtained at 189 cm and at 224 cm from the ion source grid. In Fig. 5.5 is shown the typical beam profiles perpendicular to the beam axis measured at the distance of 224 cm. These profiles indicate the Gaussian distribution. The e-folding divergence angle (half width) is about 1.5 deg, which slightly changes depending on the beam energy and the current.

Figure 5.6 shows the total heat loading and the maximum heat flux to the test channel. The total heat loading was obtained calorimetrically by temperature rise of the coolant water. The maximum heat flux shows the heat flux of the surface at the center of the test section. This heat flux is considered to be directly conducted to the cooling surface because of the thin wall. The ion source worked stably with sufficient reproducibility of the beam, which was confirmed by the photo beam monitor.

For the protection of the tube wall against damage due to burnout, the ion beam was stopped automatically when surface temperature rose above a preset value of about 500 °C. This enabled us to obtain many data from a single test channel, thereby minimized aging effect of the channel.

The experiment was conducted at a beam energy of 70 kV, in the flow velocity of 3 to 7.5 m/s, exit pressure of 0.4 to 1 MPa and subcooling of 30 to 80 deg at the burnout point. The inlet temperature of coolant water was 20 °C.

5.3 RESULTS AND DISCUSSION

(1) Burnout and film boiling

All the present results can be classified into three groups, manely, stable nucleate-boiling, quasi-stable film boiling and burnout. The nucleate-boiling results can be identified according to exit pressure and saturation temperature. The latter two results include informations of critical heat flux, and are examined in the following. Three examples of recorded signals are shown in Figs. 5.7-a,b and c. The curves labeled by 1 and 2 show the surface temperature at the center of the test section, and 5 cm downstream from the center, respectively. The curves 3, 4 and 5 show bulk temperature, pressure of water at the exit and the control pulse of the ion source respectively. The abscissa is time, which passes from left hand side to right. The origins of these curves are shifted each other in both horizontal and vertical directions.

In the case of Fig. 5.7-a, a test channel was bombarded by the ion beam of 4.2 A at 70 kV, where the flow velocity was 3.2 m/s and the exit pressure 0.93 MPa. The surface temperature 1 rises to the equilibrium value of 290 °C within 1 sec (refers to the time after the beam initiation hereafter), and the temperature 2 reaches 250 °C. In this equilibrium state, the wall temperature was determined by saturation temperature. The temperature 1 begins to fluctuate at 1.5 sec owing probably to formation of vaper layer, which seems to reach the point of 5 cm downstream at 2.5 sec. This temperature begins to rise very quickly at 2.0 sec and the hot region also spreads to reach the point of 5 cm downstream at 3.7 sec. Water temperature rises as high as 140 °C and begins to decrease after 4.7 sec. This decrease may show an reduction of heat transfer due to burnout.

This result may indicate that overheating of the wall surface led to dry-out of a narrow region in an early stage of vapor layer formation, and the resultant hot spot expanded being preceded by the vapor layer. The ion beam was stopped at 5.2 sec owing to water leakage from a pinhole made by burnout at the center of the test section. There was concavely melted region of about 1 cm width and 2 cm length on the surface. The large amplitude of the fluctuation in the pressure is attributable to the failure in degassing the pressure tap. In the other cases, the fluctuation in the pressure was small as shown in Figs. 5.7-b and c. No

appreciable change in the flow rate was observed owing to turn ON and OFF of the ion beam. Large impulses on the curves 4 and 5 at 5.7 sec are noises due to electrical breakdown from the acceleration power supply of the ion source.

For higher velocity, the excursion of the surface temperature takes place slowly as shown in Fig. 5.7-b, where the velocity was 7.4 m/s and the exit pressure 0.41 MPa. The test channel was heated by the ion beam of 5 A at 70 keV. The surface temperature 1 rises rapidly up to 400 °C within 2 sec, relatively slowly from 2 sec to 7.5 sec, and begins excursion at 7.5 sec. The temperature 2 once reaches 270 °C, and rises gradually after 3.0 sec. This temperature begins excursion at 7.7 sec, which is only 0.2 sec after the excursion in the temperature 1. The hot region seems to expand very quickly. This fact, together with the higher surface temperature by about 200 °C than the saturation temperature, may indicate that the vapor layer grew wide and thick, to the point where it greatly reduce enthalpy transport between the subcooled liquid core and the superheated liquid wall layer.

The ion beam was interrupted for a very short time at 8.5 sec and at 10.2 sec by the interlocking signal with the surface temperature and was stopped at 10.6 sec by the preset sequence timer.

When the heat flux was adjusted to be a little lower than the burnout heat flux, the signals from the test section changed as shown in Fig. 5.7-c, where the velocity was 6.4 m/s and the pressure 0.59 MPa. The applied ion beam was 4.85 A at 70 keV. The temperature 7 rises to 370 °C within 1.2 sec, and gradually approaches the quasi equilibrium temperature at about 400 °C. The temperature 2 once rises to equilibrium point at 270 °C and begins to fluctuate from 270 °C to about 340 °C after 1.2 sec. This fluctuation may be caused by a thick vapor layer fluctuating in size. A small increase or decrease of the heat flux settled the temperature at about 340 °C or 270 °C, respectively. In what follows, those cases where the surface temperature reached quasi-stable state at about 400 °C like Fig. 5.7-c, where mentioned as film boiling.

Burnout and film boiling results as a function of flow velocity is shown in Fig. 5.8, where pressure is held constant at 0.59 MPa. The ordinate denotes the maximum heat flux indicated in Fig. 5.6 and the abscissa flow velocity. The filled circles show burnout, the open circles film boiling, and the solid and broken lines their boundaries. Burnout and film boiling heat fluxes increase with flow velocity. The film

boiling region which appears more than 4.5 m/s of the velocity, spreads with an increase of the velocity indicating that a vapor layer is more stable at higher velocity.

At high flow velocities (more than 5 m/s), probability of burnout can be minimized. This is because at high velocities, (1) burnout heat flux is high, (2) it takes long period from the beam initiation to the breakout of burnout, which is comparable to the operation period of 10 sec, and (3) ion beam can be stopped before breakout of burnout by measuring the surface temperature rise due to film boiling by means of infrared photography. However, comparing the cases of Figs. 5.7-a and b, shows that damage caused by burnout will be greater in the case of higher velocity than lower velocity.

(2) Burnout data and correlations

Burnout results are compared with the Zenkevich equation[12],

$$q = L\sqrt{\frac{\sigma\rho_\ell V_\ell}{\nu_\ell}}\ (2.5 + 184\ \frac{i_{\ell s} - i_\ell}{L}) \times 0.42 \times 10^{-7} \qquad (1)$$

in Fig. 5.9. The ordinate shows the ratio of the burnout heat flux to that obtained from eq.(1), and the abscissa non-dimensional subcooling $(i_{\ell s} - i_\ell)/L$. All results are presented in terms of the local values. While the present results appear to agree with the equation at low subcooling, they rapidly deviate to give smaller heat flux with an increase of subcooling. This tendency appears to be independent of pressure and flow velocity. For the clarification of the sensitivity to subcooling, these data are plotted as shown in Fig. 5.10. The ordinate corresponds to the non-dimensional heat flux defined by $(q/L)\sqrt{\nu_\ell/\sigma\rho_\ell V_\ell}$, and the abscissa the non-dimensional subcooling $(i_{\ell s} - i_\ell)/L$. The data fall on a horizontal line, which indicates that the present burnout heat flux is insensitive to subcooling. The solid lines in Figs. 5.9 and 5.10 show the average value over the data for the A-type tube, and express them with accuracy of ±12 %. The line gives the correlation,

$$q = L\sqrt{\sigma\rho_\ell V_\ell/\nu_\ell} \times 15 \times 10^{-7} \times 0.42\ (MW/m^2) \qquad (2)$$

This correlation means that the burnout heat flux depends mainly on the flow velocity and is less sensitive to pressure than the physical

parameters are. Burnout heat fluxes for the B-type tube generally fall slightly lower than those for the A-type tube. This may be an effect of the wall thickness.

Heat fluxes for the film-boiling were shown in Fig. 5.11, where the notations are the same as those in Fig. 5.10. The solid line indicates eq.(2). These results are also insensitive to subcooling and fall within +7 % and -20 % from eq.(2).

The meaning of eq.(2) is as follows. Taking square of the both sides of eq.(2), we derive,

$$\rho_v V_v^2 d/\sigma = \text{Const} \quad (\frac{V_\ell d}{\nu})(\frac{\rho_\ell}{\rho_v}) \tag{3}$$

where, $V_v = q/\rho_v \cdot L$.

Namely, there is a critical Weber number, which is determined by the Reynolds number and the density ratio. This suggests that burnout results from blow off of the forced-convection boundary layer due to vapor stream.

The hydrodynamic condition for boundary-layer separation has been developed by Tong[13] to yield a burnout expression,

$$q = c\, L \rho_\ell V_\ell / Re^{0.6} \tag{4}$$

The coefficient c is a function of negative quality for subcooled conditions. The coefficient was calculated from the present results, and indicated in Fig. 5.12 as a function of subcooling. The broken line shows the coefficient derived by Tong. The present result again indicates insensitivity to subcooling. The solid line shows the average value of the data,

$$C = 2$$

Thus burnout heat flux is given by,

$$q = 2\, L \rho_\ell V_\ell / Re^{0.6} \tag{5}$$

This expression includes all the results for the A-type tube within ±15 %.

The relation between the present results and the Griffith's expression[14] is shown in Fig. 5.13, where the ordinate show the coefficient of Griffith F,

$$F = \frac{41.5\, q\, P_{\gamma\ell}^{2/3}}{(i_{vs} - i_e)\rho_v (g\nu_\ell)^{1/3}\, F_2} \left(\frac{\rho_\ell}{\rho_\ell - \rho_v}\right)^{\frac{1}{3}}$$

$$F_2 = 1 + 10^{-6}\mathrm{Re} + 0.0144S + 0.5 \times 10^{-3}\sqrt{\mathrm{Re}\cdot S} \qquad (6)$$

$$S = C_\ell \cdot T_{sub} \cdot \rho_\ell / L \cdot \rho_v$$

$$\mathrm{Re} = u D_\ell / \nu_\ell$$

and the abscissa the pressure. The upper and lower broken lines show the scattering width of his data which eq.(6) was obtained from. While almost all the present results fall in the band width, the results become to reach the lower line with an increase of the pressure. Hence care must be taken to use eq.(6) above the pressure of 0.9 MPa.

The relation between the results and the Gluschenko's non-dimentional correlation[15] are shown in Fig. 5.14. The ordinate donotes the ratio of the present burnout heat flux to the heat flux calculated from the experimental conditions with the expression of Gluschenko,

$$K_1 = 18.25\, K_2^{0.35}\, K_3^{0.5}\, K_4^{1.2}$$

$$K_1 = q / L \rho_v V$$

$$K_2 = C_P T_{sub} \rho_\ell / L \rho_v \qquad (7)$$

$$K_3 = K / V D C_P \rho_\ell$$

$$K_4 = L / C_P T_{sat}$$

From this figure it is clear that eq.(5) also predicts larger burnout heat flux with an increase of subcooling. Hence in order to use the expression of eq.(7) it is necessary to make corrections with the result of this figure.

5.4 CONCLUSION

The critical heat fluxes have been obtained by means of ion beam irradiation of a copper finned tube in highly subcooled forced convective boiling. These results indicated insensitivity to local subcooling as well as to pressure, and a simple correlation was derived for critical

heat fluxes of about 10 MW/m^2 with velocities of up to 7.5 m/s and pressures up to 1 MPa.

On the basis of these results, the beam dumps of the JT-60 NBI were designed to handle heat fluxes of as high as 5 MW/m^2. Under this design condition eq.(2) becomes,

$$q = 4.5 \sqrt{V} \qquad (MW/m^2)$$

For a velocity of 7 m/s this correlation gives a burnout heat flux of 12 MW/m^2, hence a safety margin of a factor of 2 for burnout.

References

1) S. Matsuda, et al., "Prototype Injector Unit For JT-60", Proc. 8th Symp on Engineering Problems of Fusion Research, San Francisco, California, Nov. (1979)
2) S. Matsuda, et al., "Conceptual Design of The JT-60 Neutral Beam Injection System", Japan Atomic Energy Research Institute Report JAERI-M 7655, May, (1977) (In Japanese)
3) T. Itoh, et al., to be submitted for publication
4) Y. Ohara, M. Akiba, Y. Arakawa, Y. Okumura and J. Sakuraba, "Electron Backstream to The Source Plasma Region in an Ion Source", J. Appl. Phys, 51(7), 3614, (1980)
5) M. Kuriyama, H. Horiike, S. Matsuda and H. Morita, "Design of Caloriemeter for JT-60 NBI", Japan Atomic Energy Research Institute Report, JAERI-M 8988, Aug. (1980)
6) M. Kuriyama, et al., to be submitted for publication
7) W.R. Gambill, "Generalized Prediction of Burnout Heat Flux For Flowing, Subcooled, Wetting Liquids", Chem. Eng. Progr. Symp. Ser., 59(41), 71, (1963)
8) A.E. Bergles, "Burnout in Boiling Heat Transfer Part II: Subcooled and Low-Quality Forced-Convection Systems", Nuclear Safety, 18(2), 154, (1977)
9) Y. Okumura, S. Matsuda, Y. Mizutani, Y. Ohara and T. Ohga, "Quasi-dc extraction of 70 keV, 5 A ion Beam", Rev. Sci. Instrum. 51(6), 728, June, (1980)
10) T. Ohga, et al., "Injector Test Stand ITS-2 for Two-Stage Ion Sources Development", Japan Atomic Energy Research Institute Report, JAERI-M 7604, March, (1978) (in Japanese)
11) M. Kawai, T. Ohga, Y. Okumura and T. Shibata, "A Multichannel Optical Beam Monitor of High Power Neutral Beams", Japan Atomic Energy Research Institute Report, JAERI-M 8778, March, (1980)
12) B.A. Zenkevich, "The Generalization of Experimental Data on Critical Heat Fluxes in Forced Convection of Subcooled Water", J. Nuc. Energy, Part B: Reactor Technology, Vol.1, 130, (1959)
13) L.S. Tong, "Boundary-Layer Analysis of The Flow Boiling Crisis", Int. J. Heat. Mass Transfer, 11(7), 1208, (1968)

14) P. Griffith, ASME Preprint No.57-HT-21: Mass. Inst. Technol. Tech. Rep. No.9, March, (1957)
W.M. Rosenow and H.Y. Choi, "Heat, Mass and Momentum Transfer", Chap.9, Prentice-Hall, Englewood Cliffs, New Jersey, (1961)

15) L.F. Glushchenko, "Correlation of Experimental Data on Critical Heat Fluxes in Subcooled Boiling", Heat Transfer-Sov. Res., 2(1), 139, Jan. (1970)

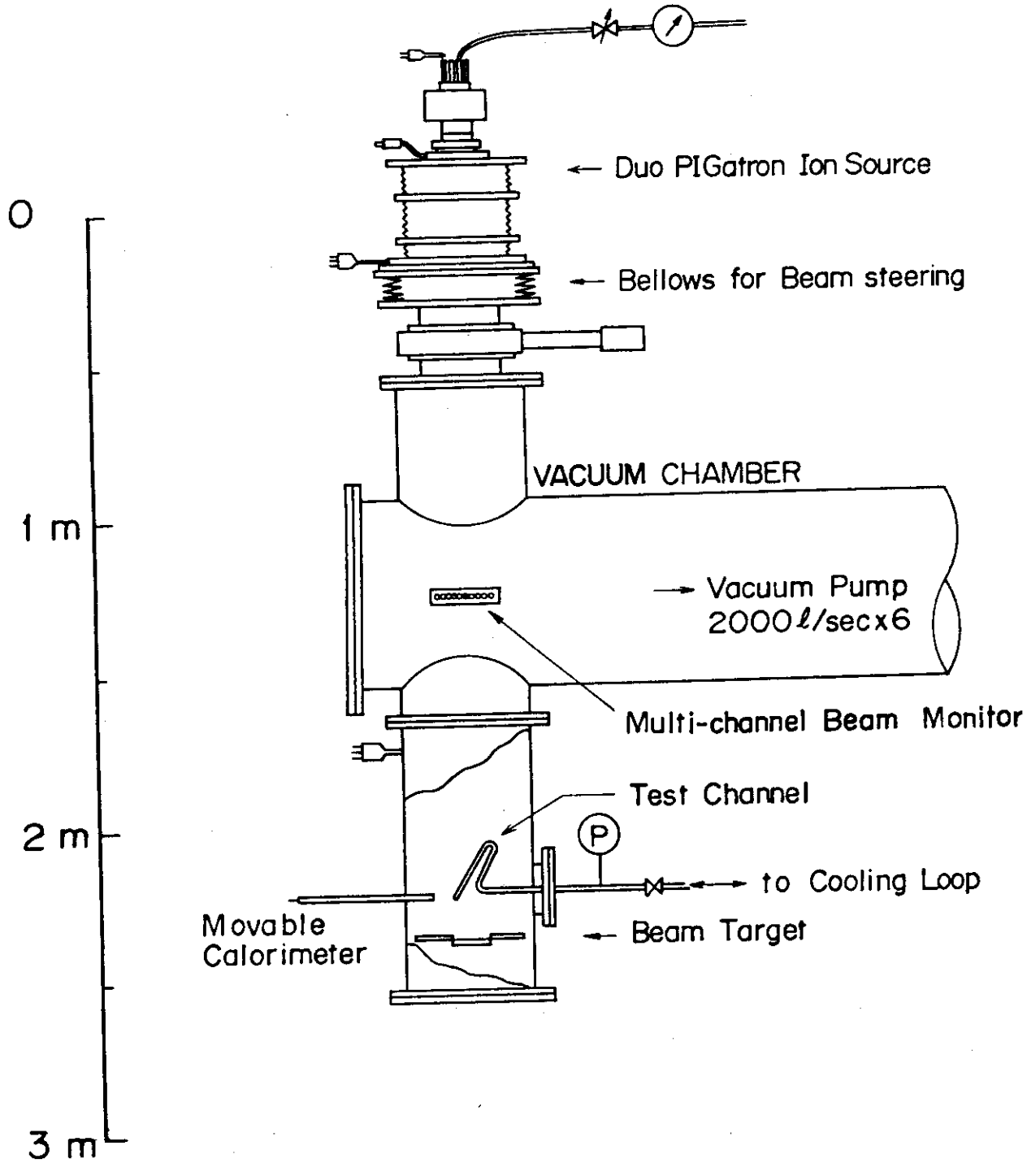

Fig.5.1 An illustration of the experimental set up.

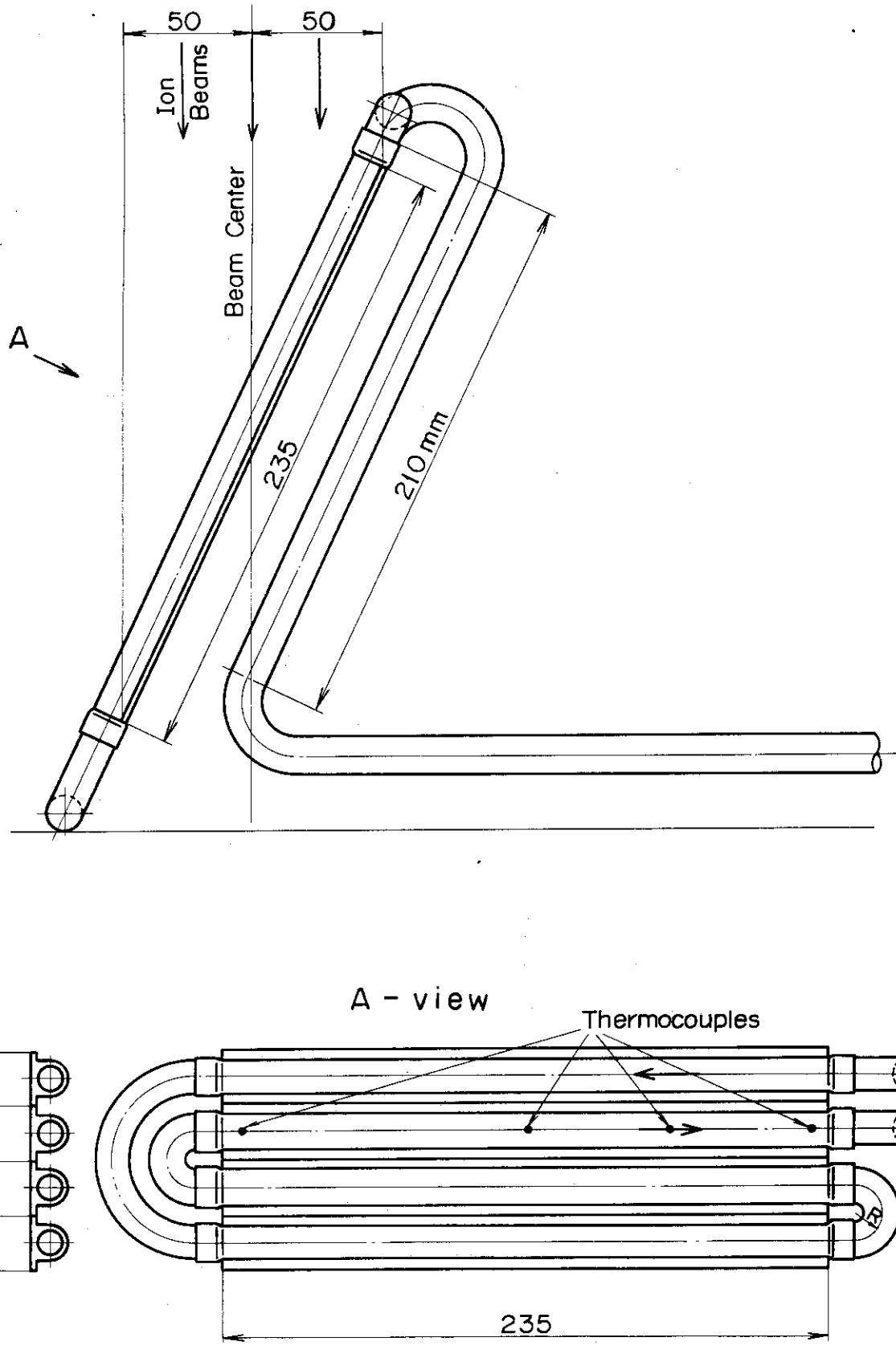

Fig.5.2 An illustration of the test channel.

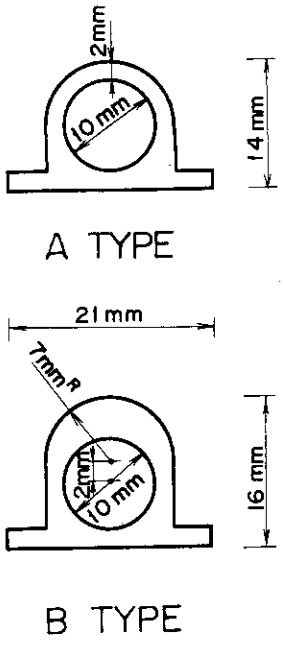

Fig. 5.3 Cross-sectional view of finned tubes.

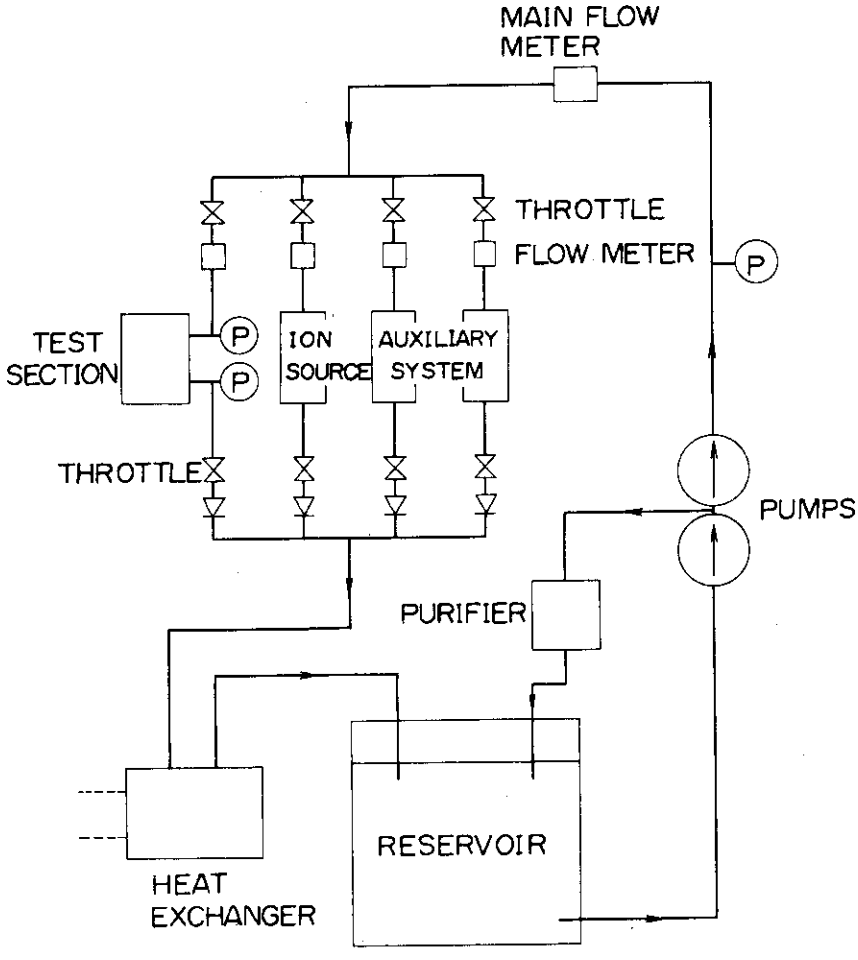

Fig. 5.4 Flow system and apparatus.

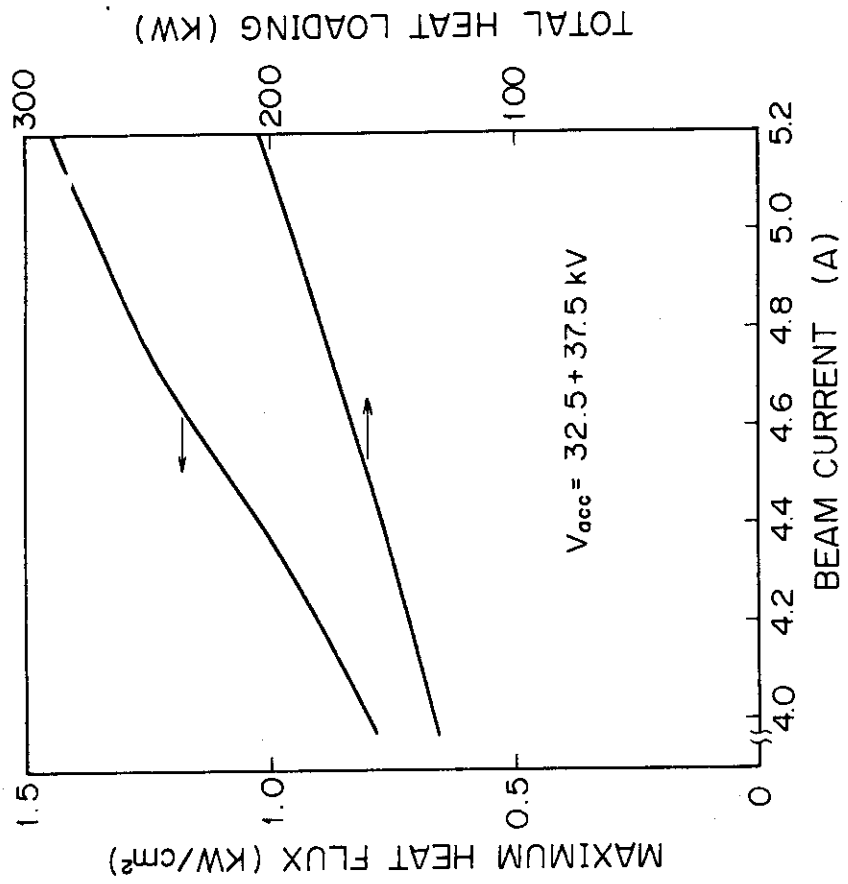

Fig.5.6 Nominal heat flux at maximum and total heat loading to the test channel.

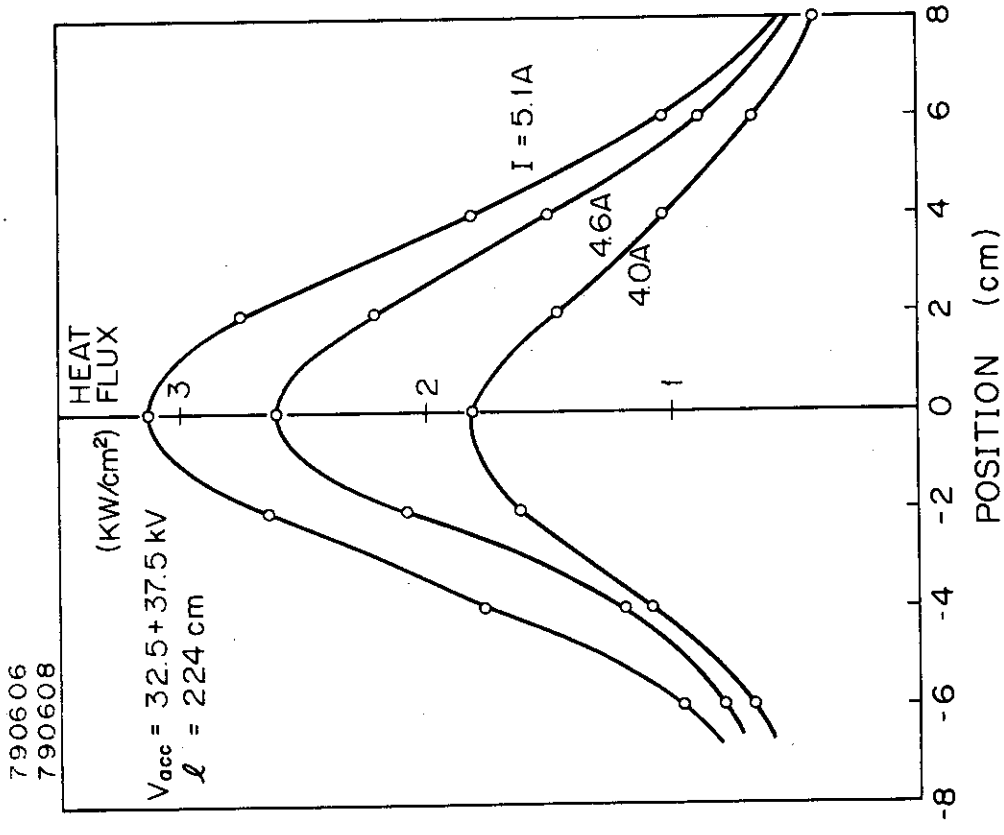

Fig.5.5 Intensity profiles of the ion beams.

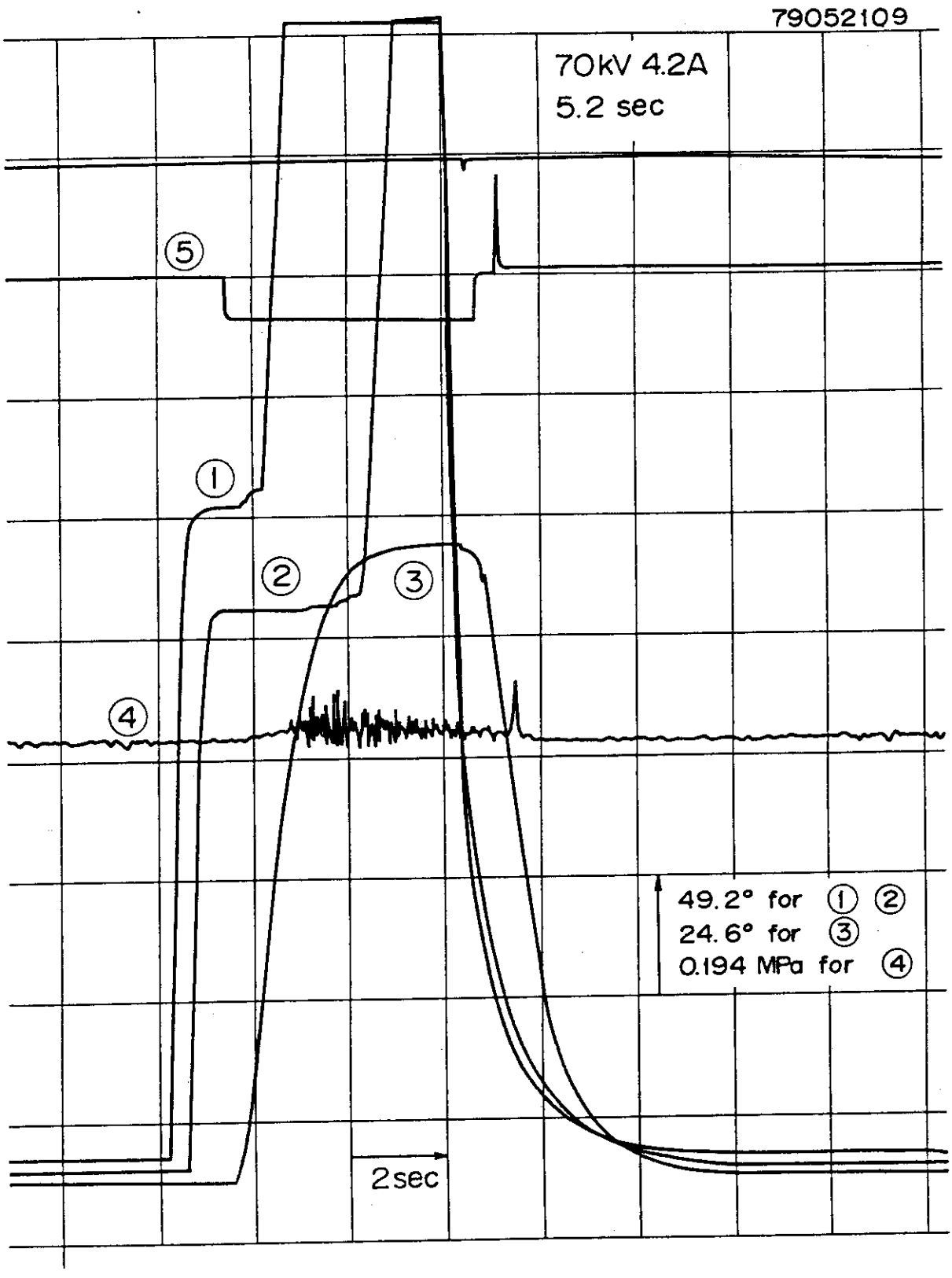

Fig. 5.7-a Temporal evolution of the surface temperatures at the center (1) and at 5 cm downstream from the center (2), water temperature (3) and pressure (4) at the exit, and the beam control pulse (5).

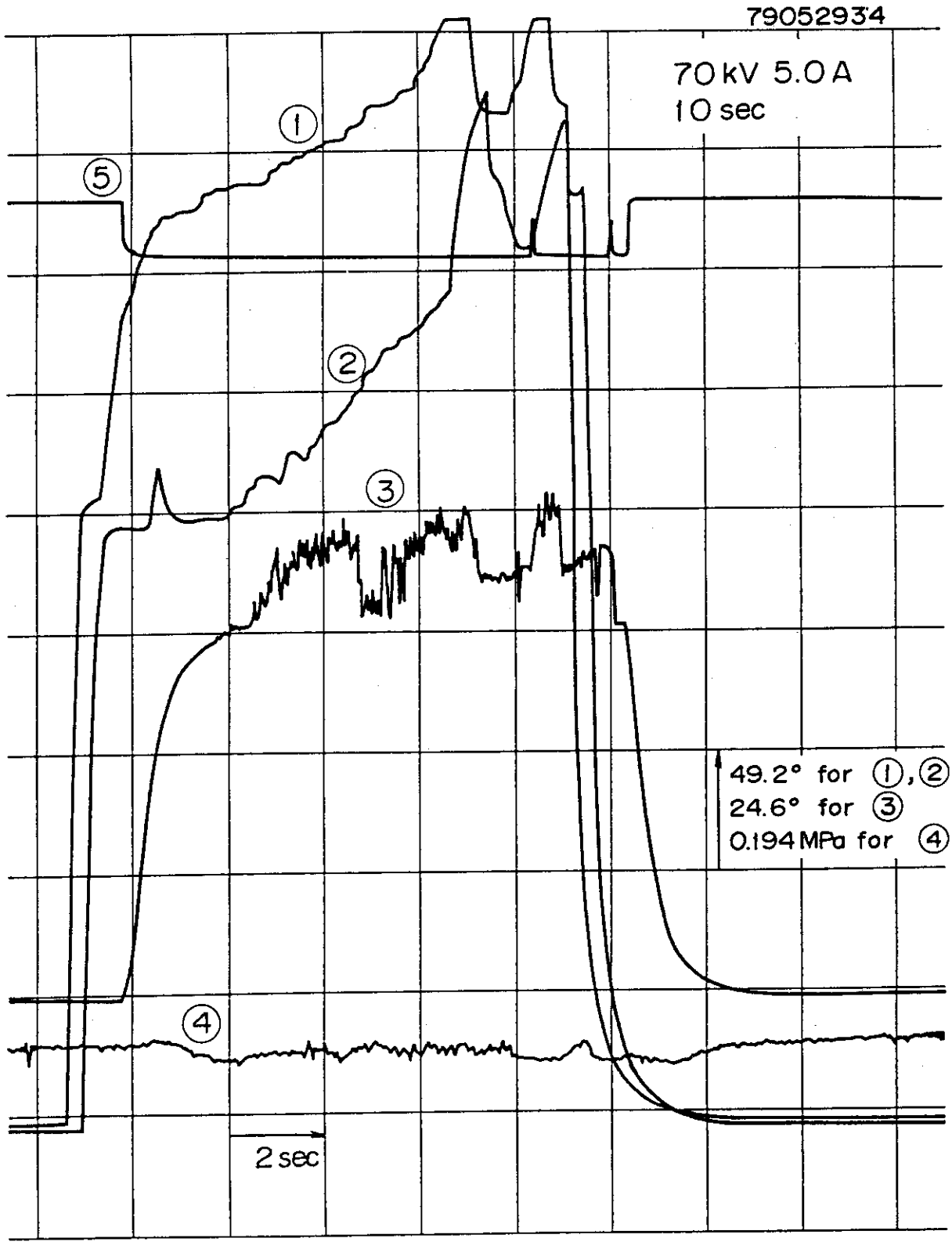

Fig. 5.7-b Temporal evolution of signals. Notations are the same as those of Fig. 5.7-a.

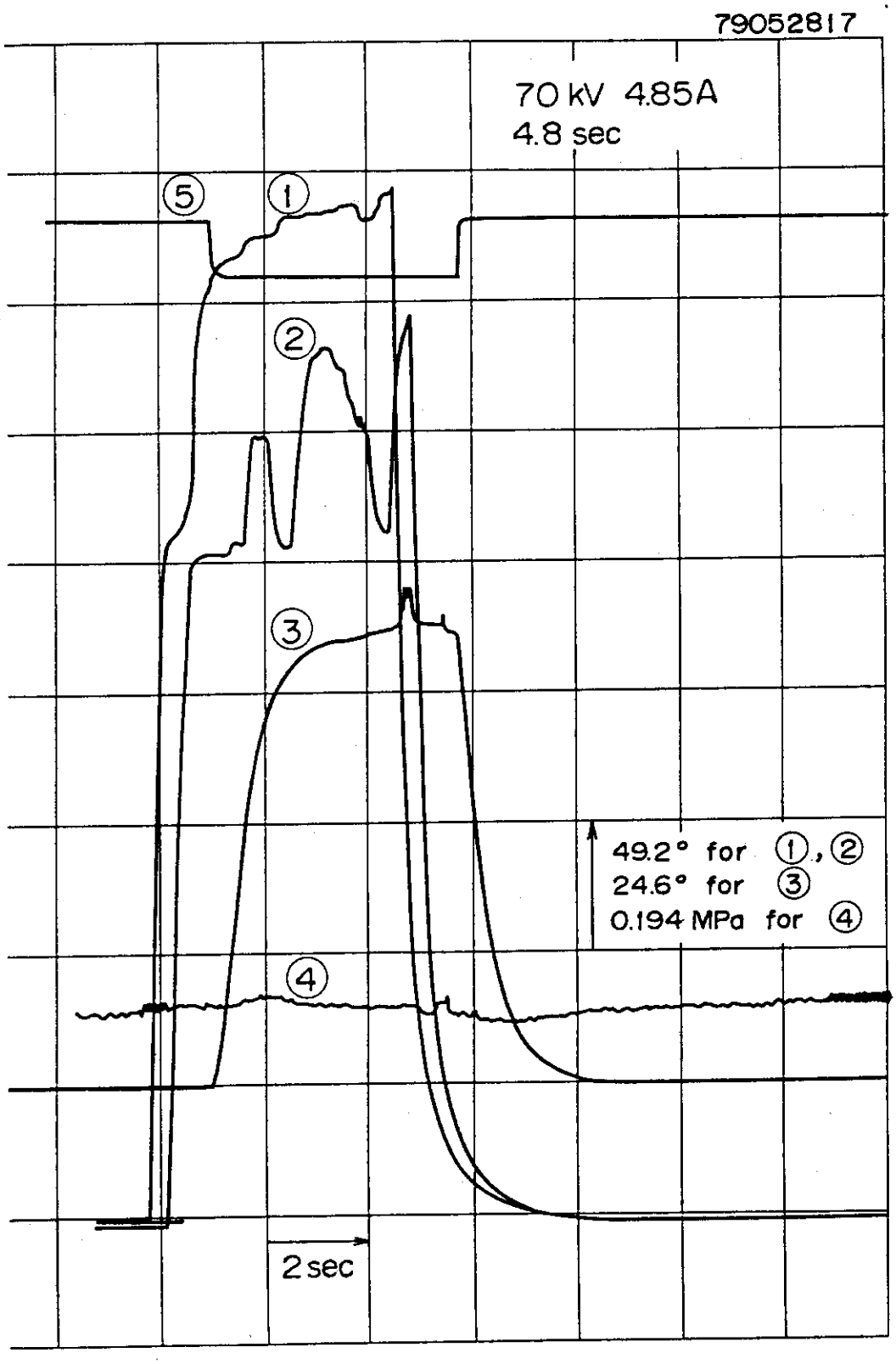

Fig. 5.7-c Temporal evolution of signals. Notations are the same as those of Figs. 5.7-a and b.

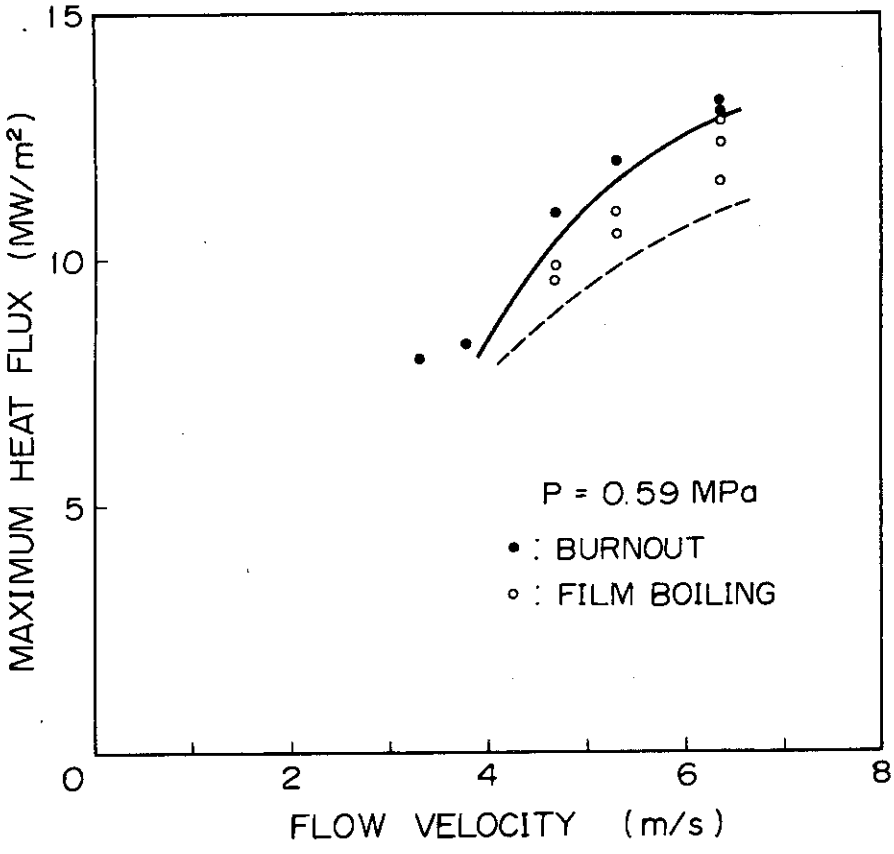

Fig.5.8 Dependence of burnout and film-boiling data on the flow velocity.

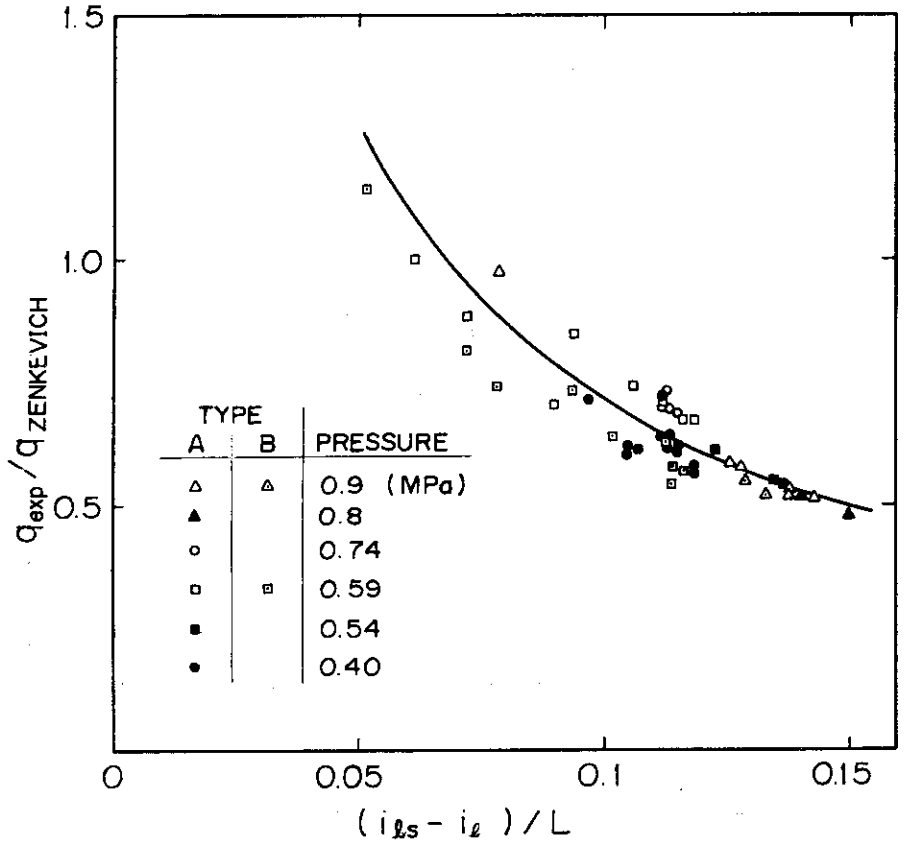

Fig.5.9 Burnout heat flux compared with Zenkevich's correlation.

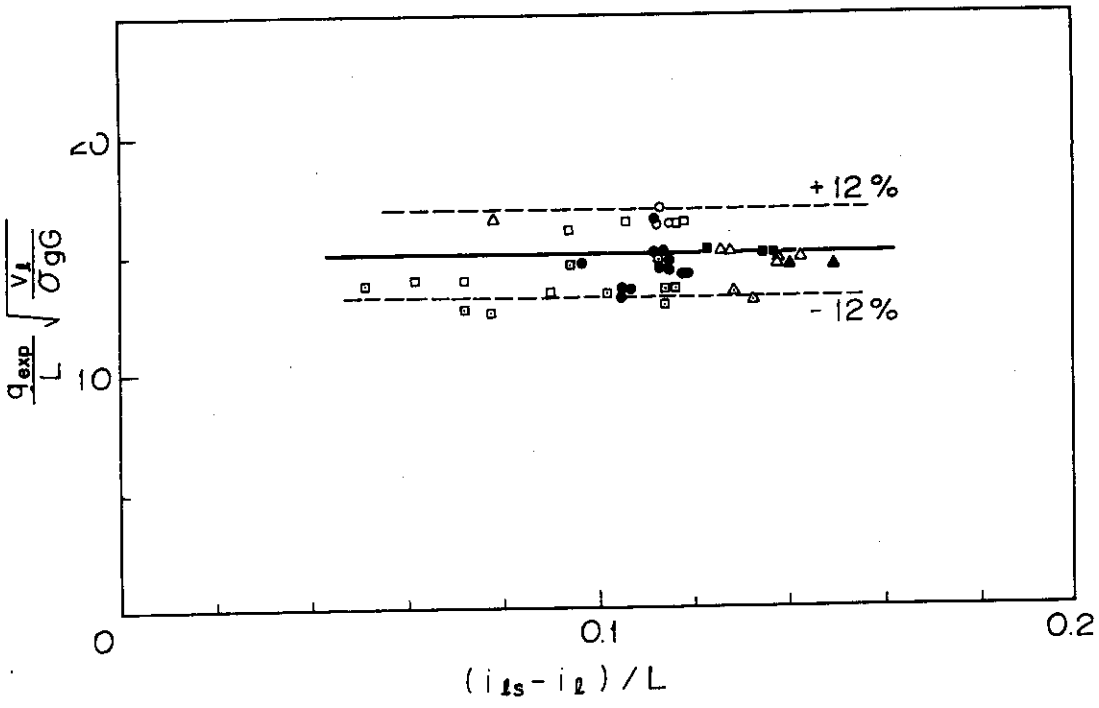

Fig.5.10 Dependence of burnout heat flux on subcooling.

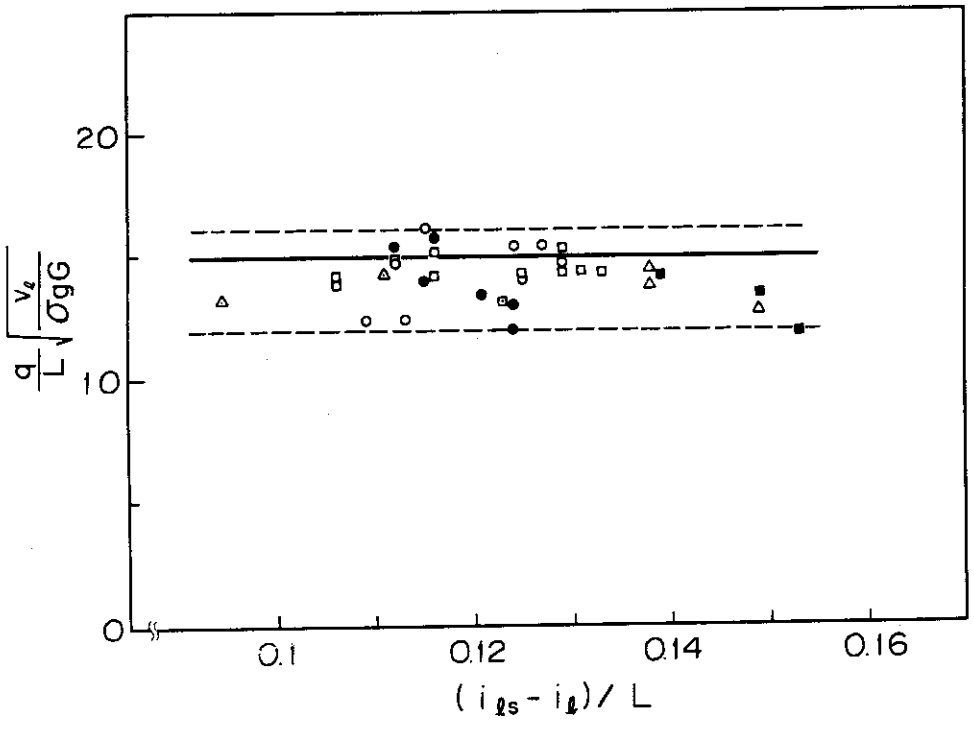

Fig.5.11 Dependence of film-boiling heat flux on subcooling.

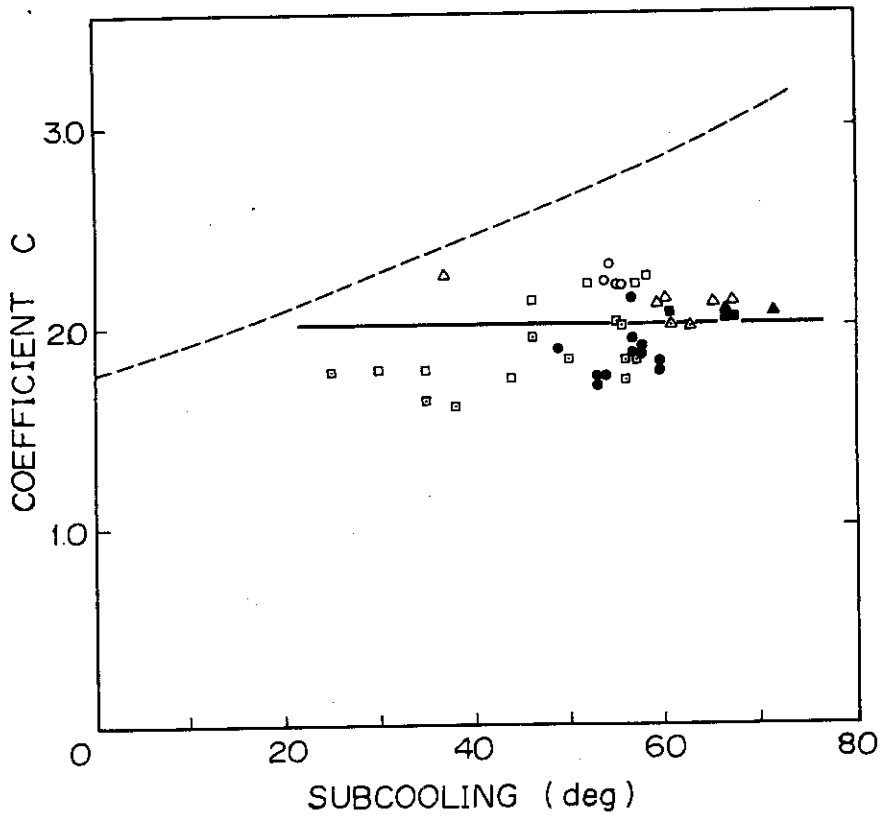

Fig.5.12 Burnout heat flux compared with Tong's correlation.

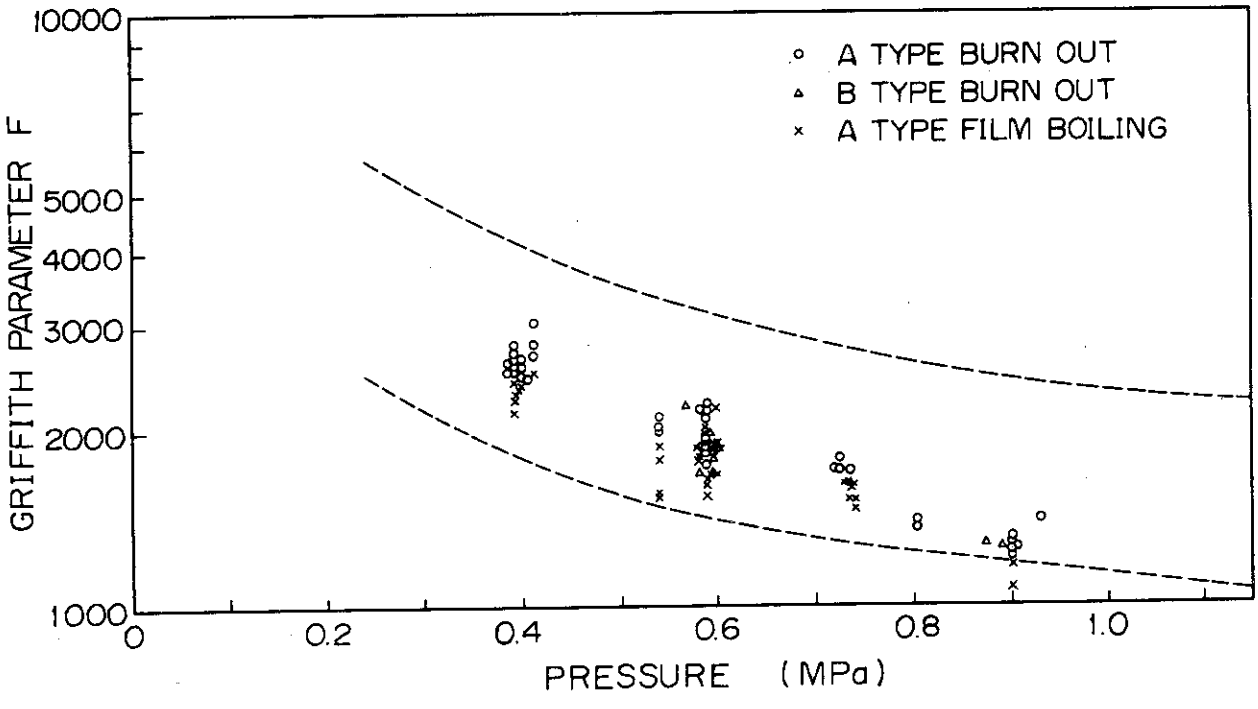

Fig.5.13 Burnout and film boiling data arranged with Griffith's correlation. The broken lines show the band width of Griffith's data.

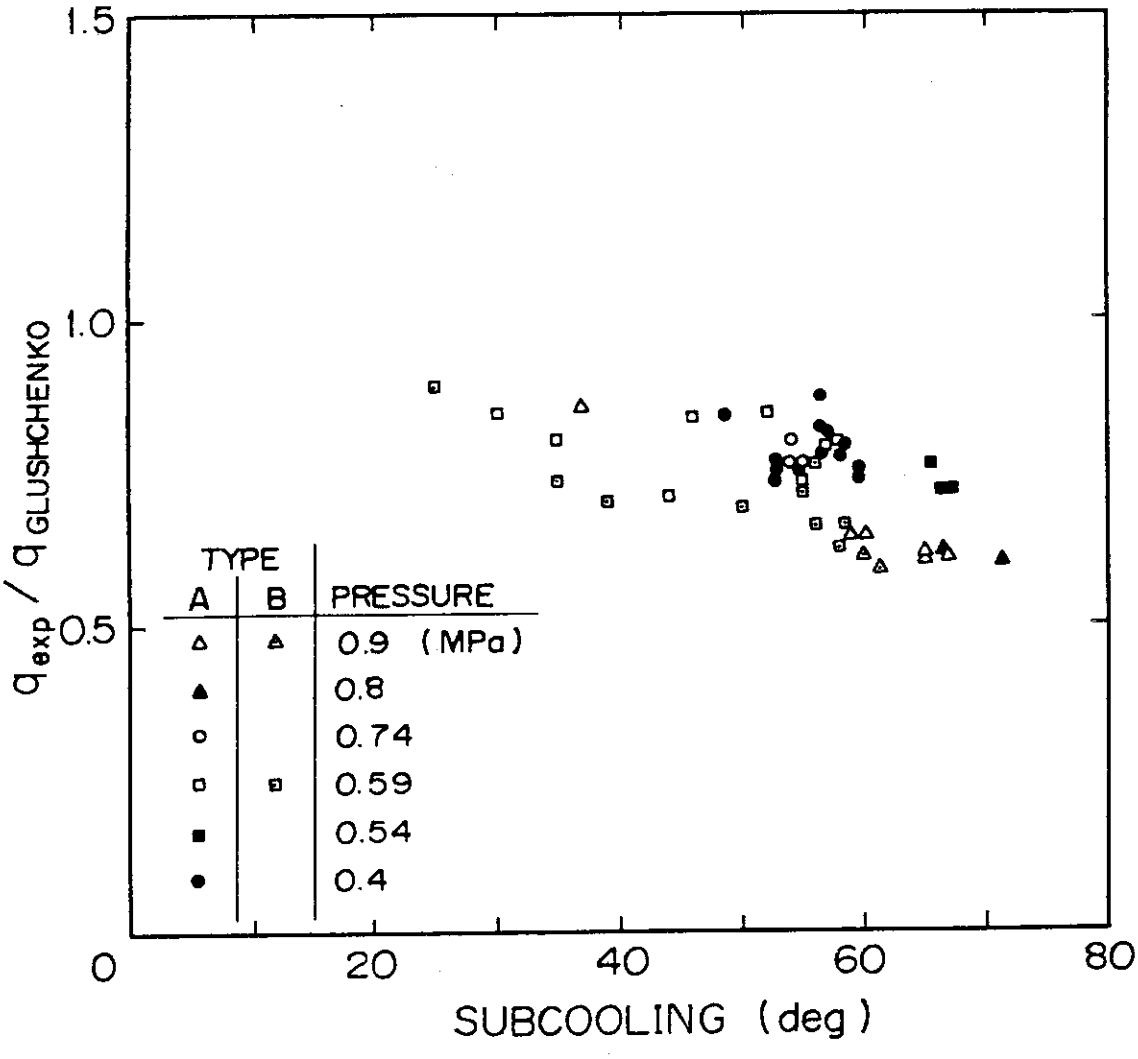

Fig.5.14 Burnout heat flux compared with Glushchenko's correlation.

In the previous chapters some of studies for the achievement of high power neutral beams for auxiliary heating of large tokamaks such as JT-60 are described. Producing large current well converged beams for long duration requires that source plasma must be dense and uniform over a large area, and that these electrode should be sufficiently cooled to maintain the initial electrostatic properties of the beam extractor for the duration. In addition, beam dumps for un-neutralized ions must withstand bombardment of the high power ion beams for long period.

For the development of reliable plasma source endurable for the long duration operation, a new variation of a duoPIGatron ion source, named coaxial duoPIGatron has been proposed and designed. This source has a magnetic center pole in the center of the intermediate electrode, thereby feeding ionizing electrons widely to the arc chamber. The first model had produced a source plasma of excellent uniformity, but the density level was low presumably due to leakage or bridging magnetic flux in the cathode plasma region. Numerical calculations have been performed on the magnetic field structure for several shapes of the intermediate electrode with center pole. The source was designed and constructed on the basis of these nuemrical results and was tested experimentally. It was confirmed that the primary electrons were fed widely to the PIG chamber along the spreading magnetic lines of force, and they produced a uniform source plasma with high density. Thus the concept of hollow feeding of electrons has proved its applicability to an ion source of larger beam extracting area.

The source generated a dense and uniform plasma over the grid of 18.5 cm diam., and produced ion beam of 30 A at 30 kV which was limited by the capacity of the high voltage power supply of the test stand. Typical operating parameters are listed in Table 3.1.

The density profile of the source plasma was not affected by the increase of applied magnetic field intensity, which shows a clear contrast with a conventional duoPIGatron case.

The coaxial intermediate electrode worked well at a fixed ratio between the center pole coil current and source coil current, indicating that the magnetic nozzle has successfully connected the cathode with source plasma region.

The arc efficiency was found to be sensitive to the effective area of the line cusp magnetic field, and to the applied magnetic field.

The efficiency, defined by the ratio of the extracted beam current to the arc power, reached 1.5 A/kW at the source coil current of 30 A when the operation of the source was most stable. The ion species fraction was measured and the proton ratio was increased to 70 % from 60 % of the modified duoPIGatron. The applied magnetic field was also effective for the production of ion beams with high proton fraction.

For the achievement of long-pulse high power beams, experimental studies were made on long duration extraction of ion beams, by means of a duoPIGatron ion source. Copper electrodes with forced water cooling pipes were tested under the condition that ion beams of 1 to 5 A at 30 kV were extracted for up to 10 sec. At the same time, a copper target that simulated an electrode of an ion source operating in a megawatt region was tested. The average heat loading to the grid area of the electrode was as high as 130 W/cm^2. This high heat flux was obtained by a set of electrodes artificially arranged to produce poor beam optics, and hence, the high heat loading. Temperature of the ground electrode was measured at two points by thermocouples buried and silver brazed in it, and was kept below 230 °C due to a large boiling heat transfer coefficient of the cooling water. No evidences of deformation or deterioration of the electrodes were observed after repetitious beam extraction. This heat loading was still a half of that on the grid of the ion source for the JT-60 NBI. However, the target experiment has demonstrated that average heat flux of as high as 570 W/cm^2 can be removed from the cooling surface of the tubes. This heat flux exceeds the requirement for the grids of the JT-60 ion source.

The other problem of heat loading, that on beam dumps was pursued experimentally for obtaining the design basis of beam dumps. A finned tube, many of which constitute the dump surface was irradiated with non-uniformly distributed hydrogen ion beams of 120 to 200 kW for up to 10 sec. The coolant water was circulated at flow velocities of 3 to 7.5 m/s at exit pressures of 0.4 to 1 MPa. The burnout and film boiling data were obtained at local heat fluxes of 8 to 15 MW/m^2. These data showed insensitivity to local subcooling as well as to pressure, and a simple burnout correlation was derived. From these results the beam dumps have been designed to recieve energetic ion fluxes of as high as 5 MW/m^2 with a margin of a factor of 2 for burnout.

ACKNOWLEDGEMENTS

The author would like to express his sincere appreciation to Professor Y. Sakurai of Osaka University for his continuous guidance and affectionate encouragement.

The author also wishes to express his appreciation to Professor M. Kawanishi, Professor T. Sekiya and Professor K. Sumita of Osaka University for their encouragement and kind advice.

The author would like to express his earnest appreciation to Professor Y. Fujii-e of Nagoya University for his continuous guidance and affectionate encouragement.

The author express his sincere gratitude to Dr. H. Shirakata for his continuous support and encouragement.

The author is most grateful to Dr. S. Matsuda for his valuable insight and suggestions to this work. He also wishes to thank Drs. Y. Arakawa and U. Kondoh for their valuable suggestions and discussions. Special thanks go to Drs. J. Sakuraba, M. Akiba, S. Tanaka, T. Sugawara, H. Morita and M. Kuriyama for their discussions and assistance in the experiments. Other members of plasma heating laboratory are gratefully acknowledged.

The author would like to acknowledge Drs. Y. Obata and S. Mori for their support and encouragement.

This study was performed at Japan Atomic Energy Research Institute as one of the works in the development of the neutral beam injector for JT-60. A part of this work was performed when the author was a JAERI research student from Osaka university.